BENDING BOUNDARY LAYERS IN LAMINATED-COMPOSITE CIRCULAR CYLINDRICAL SHELLS+

Michael P. Nemeth* and Stanley S. Smeltzer, III**
Mechanics and Durability Branch, NASA Langley Research Center
Hampton, Virginia 23681-2199

Abstract

An analytical, parametric study of the attenuation of bending boundary layers or edge effects in balanced and unbalanced, symmetrically and unsymmetrically laminated thin cylindrical shells is presented for nine contemporary material systems. The analysis is based on the linear Sanders-Koiter shell equations and specializations to the Love-Kirchhoff shell equations and Donnell's equations are included. Two nondimensional parameters are indentified that characterize and quantify the effects of laminate orthotropy and laminate anisotropy on the bending boundary-layer decay length in a very general and encompassing manner.

A substantial number of structural design technology results are presented for a wide range of laminated-composite cylinders. For all the laminate constructions considered, the results show that the differences between results that were obtained with the Sanders-Koiter shell equations, the Love-Kirchhoff shell equations, and Donnell's equations are negligible. The results also show that the effect of anisotropy in the form of coupling between pure bending and twisting has a neglible effect on the size of the bending boundary-layer decay length of the balanced, symmetrically laminated cylinders considered. Moreover, the results show that coupling between the various types of shell anisotropies has a negligible effect on the calculation of the bending boundary-layer decay length in most cases. The results also show that in some cases neglecting the shell anisotropy results in underestimating the bending boundary-layer decay length and in other cases it results in an overestimation.

Primary Symbols

$a_{12}, a_{22}, a_{26}, b_{21}$	inverted stiffness expressions defined in Appendix C
$\bar{a}_{12}, \bar{a}_{22}, \bar{a}_{26}, \bar{b}_{21}$	modified inverted stiffness expressions defined in Appendix B
$\mathcal{A}, \mathcal{A}_0$	nondimensional anisotropy parameters
$A_{11}, A_{12}, A_{16}, A_{22}, A_{26}, A_{66}$	laminate membrane stiffnesses
$\bar{A}_{16}, \bar{A}_{26}, \bar{A}_{66}$	modifed laminate stiffnesses defined in Appendix B
$B_{11}, B_{12}, B_{16}, B_{22}, B_{26}, B_{66}$	laminate membrane-bending coupling stiffnesses
$\bar{B}_{16}, \bar{B}_{26}$	modifed laminate stiffnesses defined in Appendix B
$\mathcal{C}_1$	first-order correction factor for anisotropy parameter
d, d^0	attenuation or decay lengths
$D_{11}, D_{12}, D_{16}, D_{22}, D_{26}, D_{66}$	laminate bending stiffnesses
e, e_0	stiffness coefficients
E_1, E_2	major and minor principal lamina moduli, respectively
G_{12}	lamina shear modulus
h, L	cylinder wall thickness and length
$M_x, M_\theta, M_{x\theta}$	axial and circumferential bending and twisting stress resultants, respectively
$N_x, N_\theta, N_{x\theta}$	axial, circumferential, and shear membrane stress resultants, respectively
$\mathcal{O}$	nondimensional orthotropy parameter
P(x)	loading function appearing in bending boundary-layer differential equation
Q_x, Q_θ	transverse-shear stress resultants
R	cylinder radius
Q, S, T	constant coefficients of bending boundary-layer differential equation
$\hat{T}$	modified shear stress resultant defined in Appendix B
$\mathcal{U}$	strain-energy density
w	normal-displacement component
x	axial coordinate of cylinder
ε	attenuation-length tolerance parameter
$\varepsilon_x^o, \varepsilon_\theta^o, \gamma_{x\theta}^o$	axial, circumferential, and shear membrane strains, respectively
θ	circumferential, angular coordinate
$\kappa_x^o, \kappa_\theta^o, \kappa_{x\theta}^o$	axial and circumferential bending and twisting strains, respectively
μ	constant defining different shell theories
ν_{12}	lamina major Poisson's ratio
ϕ	lamina fiber angle

+ Dedicated to the memory of Prof. J. Lyell Sanders, Jr. - a former employee of the NASA Langley Research Center.
* Senior Research Engineer. Associate Fellow, AIAA.
** Research Engineer. Member, AIAA.

Introduction

The term, "bending boundary layer," refers to localized zones of bending stresses and deformations that appear in practically every type of thin shell structure.[1] Bending boundary layers are caused by edge support conditions; by localized mechanical loads, heating, or cooling; and by abrupt changes in stiffness, such as that caused by a cutout, a crack, or a stiffener. All of these effects may be real concerns in a given preliminary design for an advanced aerospace vehicle made of laminated-composite materials. Thus, it is useful to have nondimensional parameters that characterize the effects of shell geometry and laminate orthotropy and anisotropy on the extent of bending boundary layers and that can be used to help guide the development of a design. For example, an optimal design for a pressure vessel might be one that exploits the membrane load-carrying action of a shell and minimizes zones of local bending stresses. Meaningful nondimensional parameters could be used at the preliminary design stage to identify families of laminates and material systems that exhibit relatively small bending boundary layers. Moreover, a meaningful estimate of the size of a bending boundary layer in a shell is very useful for determining an adequate first-approximation finite-element model for a complex shell structure. Without a proper understanding of the extent of a bending boundary layer, it is possible to have a finite-element model that could miss a significant part of the structural response in a region where failures are often initiated by high interlaminar stresses. Furthermore, apriori knowledge of the extent of bending boundary layers is useful in determining the instrumentation locations in structural verification tests or in material characterization tests.[2] In addition, knowledge of how laminate construction affects the extent of a bending boundary layer is useful for understanding how nonlinear prebuckling deformations affect the buckling behavior of cylindrical shells.

Studies of the behavior of axisymmetric, bending boundary layers in right-circular, cylindrical shell structures made of orthotropic or anisotropic materials and with finite length have been presented, to at least some extent, in Refs. 1 through 13. In the discussion that follows, reference is made to unbalanced and balanced laminates that are either symmetrically or unsymetrically laminated. Herein, the term unbalanced laminate is used to indicate that coupling between pure extension or contraction and shearing is present in a laminate. The term unsymmetric laminate is used to indicate coupling between any of the components of bending action with any of the components of membrane action. A fully anisotropic laminate would include both of these types of anisotropy in addition to the anisotropy that is manifested by coupling between pure bending and twisting action that is sometimes exhibited by balanced, symmetric laminates.

In Ref. 1, an analysis is presented and an expression for the attenuation or decay length of the bending boundary layer for a specially orthotropic cylinder that is subjected to edges loads, internal pressure, and heating is given. These equations, and the accompanying results, are based on the linear Love-Kirchhoff shell equations. In Ref. 3, an analytical solution that is based on Donnell's simplifications to the linear Love-Kirchhoff shell equations is given for fully anisotropic cylinders that are subjected to lateral pressure and edge loads. Results that show the effect of laminate anisotropy on the edge moment are presented for a clamped two-ply shell that is subjected to internal pressure. In addition, a discussion is presented that suggests that solutions that are based on Donnell's equations should be accurate for laminates that are not highly anisotropic. An analytical study of bending boundary layers in unbalanced, symmetrically laminated cylinders, that is also based on Donnell's equations, is presented in Ref. 2. The aim of this study was to determine a suitable gage section in a laminated-composite tube that is to be used for a material characterization test. Results are presented for unidirectional, helical-wound tubes.

An analytical solution for bending boundary layers in unbalanced, symmetrically laminated and balanced, unsymmetrically laminated circular cylindrical shells that are subjected to internal pressure and thermal loads is presented in Ref. 4. The solution is also based on Donnell's linear equations and numerical results are presented for filament-wound cylinders made of heat-treated carbon-carbon material. A study that focuses mainly on prebuckling deformations, with bending boundary layers, in homogeneous, orthotropic and unsymmetrically laminated cross-ply cylinders that are subjected to axial-compression loads and lateral pressure loads is presented in Ref. 5. The effects of the bending boundary layers on the buckling response are examined for several laminate constructions, but the general effects of the laminate construction on the extent the boundary layers are not discussed.

A pair of complex conjugate, fourth-order equations that are based on Flugge's corresponding equations[14] and that can be solved in closed form are derived for specially orthotropic, circular cylindrical shells in Ref. 6. Moreover, eigenfunction solutions are presented that include the solution for the axisymmetric bending boundary layer and several simplifed equations are presented and their relative accuracy is analyzed. In Ref. 7, a study of bending boundary layers in transversely isotropic circular cylindrical shells is presented. This study examines the attenuation characteristics of bending

boundary layers by applying an asymptotic method to the linear, three-dimensional elasticity equations, and presents order-of-magnitude estimates for the stresses and displacements for a wide range of ratios of the two principal elastic moduli. In Ref. 8, an analytical solution for an unbalanced, unsymmetrically laminated circular cylindrical shell that is subjected to internal pressure is presented that is based on a variant of the Love-Kirchhoff shell theory, which uses an expression for the change in surface twist that was given by Timoshenko. Numerical results are also presented for a two-ply shell that demonstrate the coupling effects of the shell anisotropies.

The bending boundary layers of an unbalanced, unsymmetrically laminated circular cylindrical shell that is subjected to axial compression, torsion, or thermal loading are investigated in Ref. 9. Results are also presented that demonstrate the coupling effects of the shell anisotropies. In addition, results are presented for two more conventional unsymmetric laminates and a typical quasi-isotropic laminate. In Refs. 10 and 11, bending boundary layers are also examined for balanced, symmetrically laminated and balanced, unsymmetrically laminated cylindrical shells, in the context of nonlinear prebuckling deformations that occur as a result of compression and thermal loads. In particular, the effects of laminate stacking sequence on the extent and character of the bending boundary layers are presented for two groups of three similar laminates. Two of the laminates are unsymmetric. In Ref. 12, a linear analysis is presented that focuses mainly on balanced, symmetrically laminated cylinders, and an expression is given for the length of the bending boundary layers near the cylinder ends that is based on the Love-Kirchhoff shell equations.

Most recently, Goldenveizer's static-geometric duality principle[15] has been used in Ref. 13 to reduce the Sanders-Koiter equations[16,17] for fully anisotropic, right-circular cylindrical shells to two coupled fourth-order equations that use a stress and a curvature function as the unknown, primary field variables. The reduction is done by adding certain negligibly small terms to the stress-strain relations, which are intrinsically in error because they must be established experimentally. The approach demonstrates how the static-geometric duality principle can be used to reduce greatly the amount of algebra needed to obtain results. Eigenfunction solutions are also presented for specially orthotropic cylinders that are in agreement with corresponding results presented in Ref. 6. Moreover, asymptotic formulas that can be used to determine axisymmetric bending boundary layer attenuation lengths and the decay of other unsymmetric, self-equilibrated edges loads are given.

With the exception of Ref. 13, explicit expressions for estimating the size of axisymmetric bending boundary layers in fully anisotropic, right-circular cylinders are not found in the literature. Moreover, there appears to be even fewer results for laminated-composite shells made of contemporary material systems and essentially no substantial parametric studies. The present paper focuses on developing meaningful estimates of attenuation lengths of bending boundary layers in balanced and unbalanced, symmetrically and unsymmetrically laminated circular cylinders. The analysis is based on the linear Sanders-Koiter shell equations and contains the Love-Kirchhoff shell equations[1] and Donnell's equations[1] as special cases, and is somewhat similar to the analyses presented by Reuter[4] and Chaudhuri, et. al.[8] With these equations, explicit expressions are obtained and nondimensional parameters are presented that characterize the effects of cylinder geometry and laminate construction on the size of a bending boundary layer in a very general manner. In particular, generic design curves are presented that use the nondimensional parameters to show the effects of laminate orthotropy and anisotropy on the attenuation length in a concise and encompassing manner. In addition, values of these parameters are presented for a very wide range of orthotropic and anisotropic laminate constructions. Also, differences in the results that were obtained in the present study by using the Sanders-Koiter shell equations, the Love-Kirchhoff shell equations, and Donnell's equations are discussed.

Analysis

The ordinary differential equation that governs the axisymmetric bending behavior of a right-circular cylinder that is subjected to edge loads or displacements and surface tractions is obtained by first specializing the linear Sanders-Koiter shell equations, that are given in Appendix A, for axial symmetry. For the equations presented herein, x and θ denote the axial and circumferential coordinates of a right-circular cylinder, respectively, and the specialization to axial symmetry is obtained by eliminating all terms in the equations that are differentiatied with respect to the circumferential coordinate, θ. The resulting set of equations for axisymmetric behavior are given in Appendix B. The ordinary differential equation that governs the axisymmetric bending behavior of a right-circular cylinder that is subjected to edge loads or displacements and surface tractions is derived in Appendix B and is given by

$$\frac{d^4w}{dx^4} + 4S\frac{d^2w}{dx^2} + 4Qw = P(x) \qquad (1)$$

where S, Q, and P(x) are defined in Appendix B by Eqs. (B55), (B56), and (B57), respectively, and w(x) is the radial deflection that is positive-valued when outward.

The coefficients of Eq. (1) depend on the subscripted A, B, and D constitutive terms of classical Love-Kirchhoff-type laminated shell theory (e.g., see Ref. 18, pp. 190-202) and the radius of the cylinder middle surface, R.

To determine the specific form of the solution to Eq. (1), it is useful to examine the positive-definiteness conditions on the strain-energy density function. The strain energy density function for this problem is given by

$$2\mathcal{U} = N_x\varepsilon_x^o + N_\theta\varepsilon_\theta^o + N_{x\theta}\gamma_{x\theta}^o + M_x\kappa_x^o + M_{x\theta}\kappa_{x\theta}^o \qquad (2)$$

where N_x, N_θ, and $N_{x\theta}$ are the membrane stress resultants; M_x and $M_{x\theta}$ are bending stress resultants; ε_x^o, ε_θ^o, and $\gamma_{x\theta}^o$ are the middle-surface membrane strains; and κ_x^o and $\kappa_{x\theta}^o$ are are middle-surface bending strains. By using Eqs. (B22), (B23), and (B28), the strain-energy density function is expressed as

$$2\mathcal{U} = N_x\varepsilon_x^o + N_\theta\varepsilon_\theta^o + \hat{T}\gamma_{x\theta}^o + M_x\kappa_x^o \qquad (3)$$

The strain energy density is expressed in terms of the strains and constitutive terms by using the constitutive equation given by Eq. (B29); that is,

$$\mathcal{U} = \frac{1}{2}\begin{Bmatrix}\varepsilon_x^o\\ \varepsilon_\theta^o\\ \gamma_{x\theta}^o\\ \kappa_x^o\end{Bmatrix}^T\begin{bmatrix}A_{11} & A_{12} & \bar{A}_{16} & B_{11}\\ A_{12} & A_{22} & \bar{A}_{26} & B_{12}\\ \bar{A}_{16} & \bar{A}_{26} & \bar{A}_{66} & \bar{B}_{16}\\ B_{11} & B_{12} & \bar{B}_{16} & D_{11}\end{bmatrix}\begin{Bmatrix}\varepsilon_x^o\\ \varepsilon_\theta^o\\ \gamma_{x\theta}^o\\ \kappa_x^o\end{Bmatrix} \qquad (4)$$

The stiffness terms in Eq. (4) that have overbars are defined by Eqs. (B31) - (B35) and are functions of the shell wall thickness-to-radius parameter, h/R. By enforcing positive definiteness of the strain energy density function (e.g., see Ref. 19), the requirement that the diagonal terms A_{11}, A_{22}, $\bar{A}_{66}$, and D_{11} be positive-valued is obtained. Moreover, the following determinants are positive valued

$$\begin{vmatrix}A_{11} & A_{12}\\ A_{12} & A_{22}\end{vmatrix} = A_{11}A_{22} - A_{12}^2 > 0 \qquad (5)$$

$$\begin{vmatrix}A_{11} & A_{12} & \bar{A}_{16}\\ A_{12} & A_{22} & \bar{A}_{26}\\ \bar{A}_{16} & \bar{A}_{26} & \bar{A}_{66}\end{vmatrix} = \left(A_{11}A_{22} - A_{12}^2\right)\bar{A}_{66} -$$

$$A_{11}\bar{A}_{26}^2 - A_{22}\bar{A}_{16}^2 + 2A_{12}\bar{A}_{16}\bar{A}_{26} > 0 \qquad (6)$$

Likewise, positive definiteness of the strain energy density function also requires that the determinant of the constitutive matrix in Eq. (4) be positive-valued. Moreover, by rearranging the strain energy density function into the form

$$\mathcal{U} = \frac{1}{2}\begin{Bmatrix}\varepsilon_x^o\\ \gamma_{x\theta}^o\\ \varepsilon_\theta^o\\ \kappa_x^o\end{Bmatrix}^T\begin{bmatrix}A_{11} & \bar{A}_{16} & A_{12} & B_{11}\\ \bar{A}_{16} & \bar{A}_{66} & \bar{A}_{26} & \bar{B}_{16}\\ A_{12} & \bar{A}_{26} & A_{22} & B_{12}\\ B_{11} & \bar{B}_{16} & B_{12} & D_{11}\end{bmatrix}\begin{Bmatrix}\varepsilon_x^o\\ \gamma_{x\theta}^o\\ \varepsilon_\theta^o\\ \kappa_x^o\end{Bmatrix} \qquad (7)$$

the following additional positive-definiteness condition is obtained

$$\begin{vmatrix}A_{11} & \bar{A}_{16}\\ \bar{A}_{16} & \bar{A}_{66}\end{vmatrix} = A_{11}\bar{A}_{66} - \bar{A}_{16}^2 > 0 \qquad (8)$$

The homogeneous solution for Eq. (1) involves the square root of the quantity $Q - S^2$. By using Eqs. (B55) and (B56), this quantity is given by

$$Q - S^2 = \frac{4C_1C_3 - C_2^2}{16C_1^2} \qquad (9)$$

Substituting Eqs. (B41) - (B43) into Eq. (9) and simplifying, the quantity $Q - S^2$ is found to be given by

$$Q - S^2 = \frac{1}{4C_1^2}\begin{vmatrix}A_{11} & A_{12} & \bar{A}_{16} & B_{11}\\ A_{12} & A_{22} & \bar{A}_{26} & B_{12}\\ \bar{A}_{16} & \bar{A}_{26} & \bar{A}_{66} & \bar{B}_{16}\\ B_{11} & B_{12} & \bar{B}_{16} & D_{11}\end{vmatrix} \qquad (10)$$

It follows logically, that $Q - S^2 > 0$ because the positive-definiteness of the strain energy density function requires that the determinant in Eq. (10) be positive valued. Moreover, $Q - S^2 > 0$ implies that $Q > 0$, and $Q > 0$ implies that $\frac{C_3}{C_1} > 0$. Equations (6), (8), and (B43) indicate that $C_3 > 0$. Thus, $\frac{C_3}{C_1} > 0$ yields the condition that $C_1 = D_{11}e > 0$ (see Eqs. (B49) and (B50)). Because $D_{11} > 0$, $e > 0$. To enunciate the positive valuedness of Q, it is convenient to introduce the expression

$$T^2 = Q = \frac{1}{4R^2\bar{a}_{22}D_{11}e} \qquad (11)$$

such that $T^2 - S^2 > 0$, and to express Eq. (1) as

$$\frac{d^4w}{dx^4} + 4S\frac{d^2w}{dx^2} + 4T^2w = P(x) \qquad (12)$$

Equation (12) is a linear, fourth-order, nonhomoge-

neous ordinary differential equation with constant coefficients. The characteristic equation of Eq. (12) is given by

$$\lambda^4 + 4S\lambda^2 + 4T^2 = 0 \tag{13}$$

Using the knowledge that $T^2 - S^2 > 0$, the roots of the characteristic equation are obtained from the quadratic formula; that is,

$$(\lambda^2)_{1,2} = 2\left(-S \pm i\sqrt{T^2 - S^2}\right) \tag{14}$$

where $i = \sqrt{-1}$. Solution of this equation for λ yields four roots of Eq. (13) that are pairs of complex conjugates that are given by

$$\lambda_{1,2,3,4} = \pm\left(\sqrt{T-S} \pm i\sqrt{T+S}\right) \tag{15}$$

The homogeneous solution of Eq. (12) can be written as follows

$$w_H(x) = K_1 e^{-\sqrt{T-S}\,x}\sin\left[\sqrt{T+S}\,x + K_2\right] + K_3 e^{-\sqrt{T-S}\,(L-x)}\sin\left[\sqrt{T+S}\,x + K_4\right] \tag{16a}$$

where $x \in [0,L]$. The symbols K_1, K_2, K_3, and K_4 are real-valued constants that are determined from the boundary conditions given by Eqs. (B18) and (B19). The solution given by Eq. (16a) represents a damped, oscillatory response that decays from each end of the cylinder. The regions near the edges of the cylinder, where the amplitude of $w_H(x)$ is the largest are called the bending boundary layers. All response quantities that exhibit bending boundary layers involve derivatives of Eq. (16a) and can be expressed in the general form

$$F(x) = F_1 e^{-\sqrt{T-S}\,x}\sin\left[\sqrt{T+S}\,x + F_2\right] + F_3 e^{-\sqrt{T-S}\,(L-x)}\sin\left[\sqrt{T+S}\,x + F_4\right] \tag{16b}$$

where F_1 through F_4 are constants.

When the length of the bending boundary layers are less than half of the cylinder length, which is typical, Eqs. (16) can be partitioned into one part that applies to the edge x = 0 and the other that applies to the edge x = L. The response quantities for the region near x = 0 are obtained by setting $F_3 = 0$ in Eqs. (16). Similarly, the response quantities for the region near x = L are obtained by setting $F_1 = 0$ in Eqs. (16).

Formulas for the Attenuation Length

Formulas for the attenuation or decay length of the bending boundary layers are obtained by first noting that the response quantities for the region near x = 0 are bounded by the two functions $\pm F_1 e^{-\sqrt{T-S}\,x}$ and that the response quantities for the region near x = L are bounded by the two functions $\pm F_3 e^{-\sqrt{T-S}\,(L-x)}$. Let d denote the length for which the solution attenuates or decays to a value of ε times the amplitude F_1 or F_3. A reasonable estimate of the attenuation length or decay length d is obtained by replacing x and (L - x) with d in the exponential terms of Eq. (16b), and by noting that the amplitude of w(x) is attenuated by the exponential terms. Thus, the attenuation length or decay length is given by $e^{-\sqrt{T-S}\,d} = \varepsilon$ which yields

$$d = -\ln\varepsilon\,(T-S)^{-1/2} < \frac{L}{2} \tag{17}$$

By using Eqs. (B55) and (11), Eq. (17) is expressed as

$$\frac{d}{\sqrt{Rh}} = \frac{d^o}{\sqrt{Rh}}\mathcal{A} \tag{18}$$

where d^o is the attenuation length, in which anisotropy is neglected, that is given in nondimensional form by

$$\frac{d^o}{\sqrt{Rh}} = -\frac{\ln\varepsilon}{\sqrt[4]{3}}\mathcal{O} \tag{19}$$

The symbol h is the shell wall thickness, and $\mathcal{O}$ and $\mathcal{A}$ are nondimensional orthotropy and anisotropy parameters or factors, respectively, that are given by

$$\mathcal{O} = \left[\frac{12\,A_{11}D_{11}}{(A_{11}A_{22} - A_{12}^2)h^2}\right]^{1/4} \tag{20a}$$

$$\mathcal{A} = \left[\frac{(A_{11}A_{22} - A_{12}^2)}{A_{11}}\,\bar{a}_{22}e\right]^{1/4}\left[1 - \frac{\bar{b}_{21}}{\sqrt{\bar{a}_{22}D_{11}e}}\right]^{-1/2} \tag{20b}$$

where the symbols in these equations are defined in Appendix B.

Other useful forms of Eq. (20a) are obtained by introducing an effective membrane Poisson's ratio $\nu_m = \frac{A_{12}}{\sqrt{A_{11}A_{22}}}$, which is the geometric mean of the two Poisson effects associated with the inplane principal direction of a homogenized orthotropic material. By using

this effective membrane Poisson's ratio, Eq. (20a) is expressed as

$$\mathcal{O} = \left[\frac{12\,D_{11}}{A_{22}h^2(1-\nu_m^2)}\right]^{1/4} \tag{21}$$

For a single-layer of homogeneous, specially orthotropic material, $\nu_m = \sqrt{\nu_{12}\nu_{21}}$, $\mathcal{A} = 1$, and

$$\mathcal{O} = \left[\frac{E_1}{E_2(1-\nu_{12}\nu_{21})}\right]^{1/4} \tag{22}$$

which, when substituted into Eq. (19), yields results identical to the results presented by Kraus[1], where the decay tolerance is given by $\varepsilon = e^{-\pi}$. Likewise, for a single-layer of isotropic material with an arbitrary thickness, $\nu_m = \nu$, $\mathcal{A} = 1$, and

$$\mathcal{O} = \frac{1}{\sqrt[4]{(1-\nu^2)}} \tag{23}$$

A 90%-decay length ($\varepsilon = .1$) that is a good approximation to the behavior of homogeneous, metallic shells is given by $\frac{d^o}{R} = 1.79\sqrt{\frac{h}{R}}$. Applying this formula, for example, to the Space Shuttle solid rocket booster described in Refs. 20 or 21 (R = 72 in., h= 0.5 in.) gives $d^o = 0.15\,R = 10.8$ in.

It is interesting to note that the differences between the attenuation lengths that are based on the Sanders-Koiter, the Love-Kirchhoff, and Donnell's equations appear in the coefficient e and in the symbols with overbars in Eq. (20b) for the anisotropy factor $\mathcal{A}$ (see Eqs. (B22), (B31) - (B35), and (B45) - (B49). For these equations, the Sanders-Koiter theory is given by $\mu = \frac{3}{2}$ and the Love-Kirchhoff theory is given by $\mu = 1$. Donnell's equations are given by $\mu = 0$. For isotropic and specially orthotropic cylinders, $\mathcal{A} = 1$ and the three sets of shell equations yield identical results. Similarly, for antisymmetric cross-ply cylinders ($A_{16} = A_{26} = D_{16} = D_{26} = B_{16} = B_{26} = B_{12} = B_{66} = 0$)

$$\mathcal{A} = \left[1 - \frac{B_{11}^2}{A_{11}D_{11}}\right]^{1/4}\left[1 - \frac{A_{12}B_{11}}{\sqrt{(A_{11}A_{22}-A_{12}^2)(A_{11}D_{11}-B_{11}^2)}}\right]^{-1/2} \tag{24}$$

and the three shell theories yield identical results.

Simplified Formulas for $\mathcal{A}$

For balanced, symmetrically laminated cylinders, the only anisotropic constitutive terms are D_{16} and D_{26}, and the anisotropy factor is given by $\mathcal{A} = \sqrt[4]{e}$ where

$$e = 1 - \frac{\mu^2 D_{16}^2}{A_{66}D_{11}h^2}\left[\frac{\left(\frac{h}{R}\right)^2}{1+\mu^2\left(\frac{h}{R}\right)^2\frac{D_{66}}{A_{66}h^2}}\right] \tag{25}$$

For thin-shell theories, such as the Sanders-Koiter theory and the Love-Kirchhoff theory, $\frac{h}{R} \le \frac{1}{20}$. This result suggests that a useful approximation to Eq. (25) and the anisotropy factor can be obtained from a power series expansion for small values of $\frac{h}{R}$. This process yields

$$\mathcal{A} \approx 1 - \frac{\mu^2}{4}\left(\frac{h}{R}\right)^2\frac{D_{16}^2}{A_{66}D_{11}h^2} \tag{26}$$

In this expression, $0 \le \mu \le \frac{3}{2}$ and $0 \le \frac{D_{16}^2}{A_{66}D_{11}h^2} \le 1$. Thus, the approximate formula for $\mathcal{A}$ indicates that for most practical applications of thin-shell theory, the differences between the three different shell theories considered herein, and the effect of the flexural anisotropy of a general symmetrically laminated cylinder, are negligible.

A simplified formula for the anisotropy factor can be derived for the general expression for $\mathcal{A}$ that is given by Eq. (20b). For this case, the following power series expansions for small values of $\frac{h}{R}$ are used

$$e = e_0 + e_1\left(\frac{h}{R}\right) + e_2\left(\frac{h}{R}\right)^2 + \cdots \tag{27}$$

$$\bar{a}_{12} = a_{12} + a_{112}\left(\frac{h}{R}\right) + a_{212}\left(\frac{h}{R}\right)^2 + \cdots \tag{28}$$

$$\bar{a}_{22} = a_{22} + a_{122}\left(\frac{h}{R}\right) + a_{222}\left(\frac{h}{R}\right)^2 + \cdots \tag{29}$$

$$\bar{a}_{26} = a_{26} + a_{126}\left(\frac{h}{R}\right) + a_{226}\left(\frac{h}{R}\right)^2 + \cdots \tag{30}$$

$$\bar{b}_{21} = b_{21} + b_{121}\left(\frac{h}{R}\right) + b_{221}\left(\frac{h}{R}\right)^2 + \cdots \tag{31}$$

Substituting Eqs. (27) - (31) into Eq. (20b) and expanding the resulting expression in a similar manner yields

$$\mathcal{A} = \mathcal{A}_0 + \mathcal{A}_1\left(\frac{h}{R}\right) + \mathcal{A}_2\left(\frac{h}{R}\right)^2 + \cdots \tag{32}$$

The coefficient $\mathcal{A}_2$ is a very complicated expression, and as a result, the following first-order approximation of $\mathcal{A}$ is used herein; that is,

$$\mathcal{A} \approx \mathcal{A}_0 \left[1 + \mu \, \mathcal{C}_1 \left(\frac{h}{R} \right) \right] \tag{33}$$

where $\mathcal{A}_0$ is the value of Eq. (20b) with $\mu = 0$, which is the anisotropy factor that corresponds to the use of Donnell's equations. This expression is given by

$$\mathcal{A}_0 = \left[\frac{(A_{11}A_{22} - A_{12}^2)}{A_{11}} \, a_{22} e_0 \right]^{1/4} \left[1 - \frac{b_{21}}{\sqrt{a_{22} D_{11} e_0}} \right]^{-1/2} \tag{34}$$

In this expression, a_{22} and b_{21} are obtained from Eqs. (B45) - (B48) by setting $\mu = 0$ in Eqs. (B31) - (B35). The expression for e_0 is obtained from Eq. (B49) in a similar manner. The term $\mathcal{C}_1$ represents a first-order correction to the results that correspond to Donnell's equations and is given by

$$\mathcal{C}_1 = \frac{\sqrt{a_{22} D_{11} e_0} \left(a_{22} e_1 + a_{122} e_0 \right) + 2a_{22} \left(b_{12} e_0 - b_{21} e_1 \right) - 2a_{122} b_{21} e_0}{4 a_{22} e_0 \left[\sqrt{a_{22} D_{11} e_0} - b_{21} \right]} \tag{35}$$

where the terms that appear in Eq. (35) are given in Appendix C. In addition, further simplifications to $\mathcal{A}_0$ and $\mathcal{C}_1$ are also presented in Appendix C for unbalanced and balanced, symmetric laminates and for balanced, unsymmetric laminates, that include the subclasses of general antisymmetric laminates, antisymmetric cross-ply laminates, and antisymmetric angle-ply laminates. The relative size of $\mathcal{C}_1$ and its contribution to Eq. (33) are examined parametrically in the subsequent section of the present study.

Results and Discussion

Equations (18) and (19) form the basis for the parametric study presented herein. In particular, the two equations isolate the contributions of shell orthotropy and shell anisotropy to the bending boundary-layer decay length with nondimensional parameters and imply the generic design-chart representations that are illustrated in Figs. 1 and 2. In Fig. 1, generic results are presented that show the nondimensional, 90%-decay length given by $\left. \frac{d}{\sqrt{Rh}} \right|_{\varepsilon = 0.1}$ as a function of the orthotropy parameter $\mathcal{O}$, for selected values of the anisotropy parameter $\mathcal{A}$. A 90%-decay length was selected herein to yield an accuracy that is approximately to within the accuracy of the experimentally determined material properties, but other values could be used.

In a manner similar to Fig. 1, Fig. 2 shows the nondimensional, 90%-decay length as a function of the anisotropy parameter $\mathcal{A}$, for selected values of the orthotropy parameter $\mathcal{O}$. Results that correspond to balanced, symmetrically laminated cylinders are given by a value of $\mathcal{A} = 1$ and results that correspond to an isotropic shell wall are indicated in the figures by the filled circle with an ordinate value of 1.79. Overall, these two figures represent results that are applicable to a vast range of laminate constructions, and provide a common basis for comparison of regular and hybrid laminates made of different material systems and laminate stacking sequences. In general, the figures show increases in the nondimensional 90%-decay length with increases in either of the orthotropy parameter $\mathcal{O}$ or the anisotropy parameter $\mathcal{A}$. In addition, the results in Figs. 1 and 2 clearly indicate the effect of neglecting shell-wall anisotropy on the attenuation length of a bending boundary layer.

The actual value of the nondimensional, 90%-decay length depends on the particular values of the orthotropy and anisotropy parameters of a given laminate. Thus, additional results are presented subsequently that show how the orthotropy parameter $\mathcal{O}$ and the anisotropy parameter $\mathcal{A}$ vary with laminate construction. In particular, values of $\mathcal{O}$ and $\mathcal{A}$ are presented first for balanced and unbalanced symmetrically laminated cylinders. Then, values are presented for balanced and unbalanced unsymmetrically laminated cylinders. Nine different contemporary material systems were used to generate these results. These material systems include boron-aluminum, S-glass-epoxy, a typical boron-epoxy, AS4/3501-6 graphite-epoxy, AS4/3502 graphite-epoxy, IM7/5260 graphite-bismaleimide, Kevlar 49-epoxy, IM7/PETI-5, and P-100/3502 pitch-epoxy materials. The mechanical properties of these material systems are presented in Table 1 and the nominal ply thickness that was used is 0.005 in.

Balanced, Symmetrically Laminated Cylinders

Symmetrically laminated shell walls are characterized mathematically by values of zero for the subscripted B terms that appear in the constitutive equation, Eq. (A15). In addition, balanced, symmetrically laminated shell walls do not exhibit coupling between extension and shear, which is characterized by $A_{16} = A_{26} = 0$ in Eq. (A15). Shell walls of this class are strictly specially orthotropic for many laminates. However, for some wall constructions, balanced, symmetric laminates exhibit anisotropy in the form of coupling between pure bending and twisting of the shell wall. This type of anisotropy is manifested by nonzero values of the D_{16} and D_{26} consti-

tutive terms in Eq. (A15). However, the discussion of Eq. (26) that has been given herein indicates that this type of anisotropy is negligible for thin shells and that the differences between results obtained from the Sanders-Koiter, the Love-Kirchhoff, and Donnell theories are insignificant. Moreover, $\mathcal{A} = 1$ for this class of laminated-composite shell walls, and the attenuation behavior is governed by the nondimensional orthotropy parameter $\mathcal{O}$ that is given by Eq. (20a). Furthermore, Eqs. (18) and (19) indicate that the attenuation length is a constant multiple of the orthotropy parameter that depends on the attenuation-tolerance parameter ε. For this case, trends that are exhibited by $\mathcal{O}$ are identical to those exhibited by the attenuation length based on any value of ε.

Values of the orthotropy parameter $\mathcal{O}$ are presented in Fig. 3 for single-ply, homogeneous, specially orthotropic and isotropic shell walls, with arbitrary thickness, as a function of the ratio of the principal elastic moduli, E_2/E_1. For these results, the orthotropy parameter is given by Eq. (22) and is expressed in the following more convenient form

$$\mathcal{O} = \left[\frac{E_2}{E_1}\left(1 - \frac{E_2}{E_1}\nu_{12}^2\right)\right]^{-1/4} \tag{36}$$

One curve, that is essentially several coincident curves, is shown in the figure that corresponds to general results for $0.2 \le \nu_{12} \le 0.35$. In addition, specific results for the nine material systems considered herein and for a typical aluminum and a steel are indicated in the figure by the square symbols. The results in Fig. 3 indicate that the effect of variations in the major Poisson's ratio on the orthotropy parameter $\mathcal{O}$ are small compared to the effect of variations in the ratio of the principal elastic moduli. Moreover, the results show that $\mathcal{O}$ decreases rapidly as the ratio of the principal elastic moduli increases, particularly for values of E_2/E_1 less than approximately 0.1, which corresponds to most of the contemporary orthotropic materials considered herein. Figure 3 also shows that an isotropic material corresponds to $\mathcal{O} \approx 1$.

Values of the orthotropy parameter $\mathcal{O}$ for the single-ply, homogeneous, specially orthotropic cylinders investigated by Cheng and He[6] were also obtained. A comparison of the results obtained in the present study with the corresponding results of Ref. 6 are presented in Table 2 for boron-epoxy, glass-epoxy, and graphite-epoxy materials and for the cylinder radius-to-thickness ratio R/h = 208.311. Moreover, a range of results is shown for Ref. 6 which corresponds to various simplifications that were used in the equations that govern the response. The actual material properties that were used are given in Ref. 6. In this table, the quantity used for comparison is given by

$$\mathcal{R}e(\mu) = \frac{\sqrt[4]{3}}{\mathcal{O}}\sqrt{\frac{R}{h}} \tag{37}$$

which is the real part of the exponent μ that appears in the eigenfunction solution used by Cheng and Ho (n = 0 in Eq. (25) of Ref. 6; see also Eq. (47) of Ref. 13), which corresponds to the decay or attenuation of the response. The orthotropy parameter shown in Eq. (37) is defined by Eq. (36). The results in Table 2, show very good agreement (less than 1% difference) for all three materials. In addition, the results obtained herein that are shown in Table 2 for the boron-epoxy material are also in excellent agreement with the corresponding results presented by McDevitt and Simmonds.[13]

Values of the orthotropy parameter $\mathcal{O}$ are presented in Fig. 4 for multilayered $[(\pm\phi)_m]_s$ laminates made from the nine material systems as a function of the fiber angle ϕ, which is measured from the x-axis toward the θ-axis. The results are independent of the stacking sequence number m and show a wide variation in $\mathcal{O}$ with the material system. The results also show, for the most part, a wide variation in $\mathcal{O}$ with the fiber angle ϕ and show a reduction in $\mathcal{O}$ as the fiber angle increases from zero to ninety degrees. The largest value (2.93) and the smallest value (0.34) of $\mathcal{O}$ are exhibited by the unidirectional laminates made from P-100/3502 pitch-epoxy material, and correspond to values of $\left.\frac{d}{\sqrt{Rh}}\right|_{\varepsilon=0.1}$ equal to 5.13 and 0.59, respectively. Moreover, the greatest variation in $\mathcal{O}$ with the fiber angle (approximately 8.7 times) is exhibited by the laminates made from P-100/3502 pitch-epoxy material. The smallest variation is exhibited by the laminates made from the boron-aluminum material.

Results are presented in Fig. 5 that show the values of the orthotropy parameter for $[(\pm 45/0_2)_m]_s$, $[(0_2/\pm 45)_m]_s$, $[(\pm 45/90_2)_m]_s$, $[(90_2/\pm 45)_m]_s$, $[(\pm 45/0/90)_m]_s$ and $[(0/90/\pm 45)_m]_s$ laminates made of IM7/5260 graphite-bismaleimide material for values of the stacking sequence number m = 1 to 6. Values of $\mathcal{O}$ range from approximately 1.53 to 0.64. These results show that the curves for the $[(\pm 45/0_2)_m]_s$ and $[(0_2/\pm 45)_m]_s$ laminates approach $\mathcal{O} \approx 1.41$ as m increases to a value of 6, with the curve for the $[(0_2/\pm 45)_m]_s$ laminates converging from above and the other curve converging from below. The higher values of $\mathcal{O}$ for the $[(0_2/\pm 45)_m]_s$ laminates, are attributed to the higher axial bending stiffness that is obtained by placing the zero-degree plies at the outer surfaces of the lami-

nates, particularly, for the lower values of the stacking sequence number m. Similarly, the results in Fig. 5 show that the curves for the $[(\pm 45/90_2)_m]_s$ and $[(90_2/\pm 45)_m]_s$ laminates approach $\mathcal{O} \approx 0.76$ as m increases to a value of 6, with the curve for the $[(\pm 45/90_2)_m]_s$ laminates converging from above and the other curve converging from below. Likewise, the results in Fig. 5 show that the curves for the $[(\pm 45/0/90)_m]_s$ and $[(0/90/\pm 45)_m]_s$ quasi-isotropic laminates approach $\mathcal{O} \approx 1.03$ as m increases to a value of 6, with the curve for the $[(0/90/\pm 45)_m]_s$ laminates converging from above and the other curve converging from below.

Overall, the results in Fig. 5 indicate that the $[(\pm 45/0_2)_m]_s$ and $[(0_2/\pm 45)_m]_s$ laminates exhibit higher values of the orthotropy parameter than the $[(\pm 45/0/90)_m]_s$ and $[(0/90/\pm 45)_m]_s$ quasi-isotropic laminates, which exhibit higher values of the orthotropy parameter than the $[(\pm 45/90_2)_m]_s$ and $[(90_2/\pm 45)_m]_s$ laminates. This trend corresponds to a reduction in the value of $\mathcal{O}$ as the axial bending and extensional stiffnesses of the laminates decrease.

Results are presented in Fig. 6 that show the effect of the nine material systems considered herein on the orthotropy parameter for the $[(0_2/\pm 45)_m]_s$ laminates. Values of $\mathcal{O}$ range from approximately 1.67 for P-100/3502 pitch-epoxy material to 1.09 for boron-aluminum material. Most of the materials exhibit values of $\mathcal{O}$ in the range of approximately 1.4 to 1.6. All of the curves show about the same reduction in $\mathcal{O}$ as the stacking sequence number m increases.

Results similar to those in Fig. 6 are presented in Fig. 7 that show the effect of the nine material systems on the orthotropy parameter for the $[(\pm 45/0/90)_m]_s$ and $[(0/90/\pm 45)_m]_s$ quasi-isotropic laminates. These results show a much smaller variation in the orthotropy parameter with material system and stacking sequence number for the quasi-isotropic laminates than for the $[(0_2/\pm 45)_m]_s$ laminates in Fig. 6. In particular, values of $\mathcal{O}$ for the quasi-isotropic laminates range from approximately 1.15 to 1. The largest values of $\mathcal{O}$ in Fig. 7 are exhibited by laminates from P-100/3502 pitch-epoxy material. Moreover, the results show a larger variation in $\mathcal{O}$ with stacking sequence number for the $[(0/90/\pm 45)_m]_s$ laminates than for the $[(\pm 45/0/90)_m]_s$ laminates.

Unbalanced, Symmetrically Laminated Cylinders

Unbalanced, symmetric laminates exhibit anisotropy in the form of extensional-shear coupling ($A_{16} \neq A_{26} \neq 0$) in addition to flexural anisotropy ($D_{16} \neq D_{26} \neq 0$). For these laminates, the value of the anisotropy parameter $\mathcal{A}$ given by Eqs. (20b) and (33) is not equal to unity. Simplifed expressions for the anisotropy parameter $\mathcal{A}_0$ and the first-order correction factor $\mathcal{C}_1$, defined by Eqs. (33) - (35), are given by Eqs. (C23) and (C24), respectively. Equation (C24) indicates that the value $\mathcal{C}_1$ depends on coupling between the membrane and flexural anisotropies.

Values of the orthotropy parameter $\mathcal{O}$ for $[(+\phi)_{2m}]_s$ symmetric, unidirectional laminates for the nine material systems considered herein are also presented in Fig. 4; that is, the curves presented in Fig. 4 for the $[(\pm\phi)_m]_s$ symmetric angle-ply laminates are identical to those for the corresponding $[(+\phi)_{2m}]_s$ symmetric, unidirectional laminates. Thus, the orthotropy behavioral trends for the unidirectional laminates are identical to those discussed previously for the symmetric angle-ply laminates, and are also independent of the stacking sequence number m.

Results for the anisotropy parameter $\mathcal{A}_0$ and the first-order correction factor $\mathcal{C}_1$ are shown in Figs. 8 and 9, respectively, for the $[(+\phi)_{2m}]_s$ symmetric, unidirectional laminates with the nine material systems considered herein and are independent of the stacking sequence number m. The results in Fig. 8 show a substantial variation in $\mathcal{A}_0$ with fiber orientation and with material system. The results show that $\mathcal{A}_0$ is the most pronounced for values of the fiber angle ϕ between approximately 55 deg and 80 deg, and that the contribution of the anisotropy to the attenuation behavior is essentially insignificant (less than 1.05) for values of $\phi < 25$ deg and $\phi > 85$ deg. Moreover, the largest variation in $\mathcal{A}_0$ with fiber angle is exhibited by the laminates made of the P-100/3502 pitch-epoxy material and the smallest variation is exhibited by the laminates made of boron-aluminum material. Values of $\mathcal{A}_0$ range from approximately 1.42 for the maximum point on the curve for the P-100/3502 pitch-epoxy material to a value of 1.

The results shown in Fig. 9 for the first-order correction factor $\mathcal{C}_1$ for the $[(+\phi)_{2m}]_s$ symmetric, unidirectional laminates indicate a substantial relative variation in $\mathcal{C}_1$ with fiber orientation and with material system, but all of the magnitudes of $\mathcal{C}_1$ are less than approximately 0.45. Moreover, the magnitude of $\mathcal{C}_1$ is less than approximately 0.2 for all of the materials except the P-100/3502 pitch-epoxy material. For the upper bound of thinness of thin-shell theory, given by h/R = 1/20, the contribution of $\mathcal{C}_1$ to the anisotropy factor defined by Eq. (33) is practically negligible. Equation (C24) indicates that the insignificance of $\mathcal{C}_1$ means that the coupling of the membrane and flexural anisotropies are negligible for these laminates. The insignificance of $\mathcal{C}_1$ is illustrated and verified in Fig. 10 for the $[(+\phi)_{2m}]_s$ symmetric, unidirectional

laminates made of IM7/5260 graphite-bismaleimide material (black curves) and made of P-100/3502 pitch-epoxy material (gray curves), for h/R = 1/20. The finely dashed curves shown in Fig. 10 correspond to 90%-decay lengths for which the anisotropy is neglected. In contrast, the solid curves and the coarsely dashed gray curve include the effect of the membrane anisotropy and are shown for values of $\mu = 0$, 1, and 1.5. For these values, results that correspond to the Sanders-Koiter theory and the Love-Kirchhoff theory are given by $\mu = \frac{3}{2}$ and $\mu = 1$, respectively. Results that correspond to Donnell's equations are given by $\mu = 0$. The solid curves in Fig. 10 for $\mu = 1$ and 1.5 are based on the exact solution that uses Eq. (20b) for the anisotropy factor. The corresponding curves that are based on the approximate formula for the anisotropy parameter that is given by Eq. (33) are identical. The solid curves and the coarsely dashed gray curve indicate that varying μ yields a small effect, which implies that all three shell theories yield essentially the same results and that $\mathcal{A} \approx \mathcal{A}_0$ for the $[(+\phi)_{2m}]_s$ symmetric, unidirectional laminates. Comparing the solid and finely dashed curves in Fig. 10 also indicates that neglecting the membrane anisotropy underestimates the bending boundary-layer decay length, by as much as approximately 31% and 21% for shell walls made of P-100/3502 pitch-epoxy and IM7/5260 graphite-bismaleimide materials, respectively.

Values of the orthotropy parameter $\mathcal{O}$ for $[(+45_2/0/90)_m]_s$ and $[(0/90/+45_2)_m]_s$ laminates made of the nine material systems considered herein are also presented in Fig. 7. More specifically, the values of $\mathcal{O}$ for these laminates are identical to the values for the corresponding quasi-isotropic laminates. Results for the anisotropy parameter $\mathcal{A}_0$ defined by Eq. (34) are shown in Fig. 11 for $[(+45_2/0/90)_m]_s$ and $[(0/90/+45_2)_m]_s$ laminates made of the nine material systems considered herein. The results in Fig. 11 show no significant variation in $\mathcal{A}_0$ with the stacking sequence number m, and only a slight variation (less than approximately 9%) with material system. Values of $\mathcal{A}_0$ range between approximately 1.1 and 1. Corresponding results for the first-order correction factor $\mathcal{C}_1$ defined by Eq. (35), that are not shown herein, were obtained that indicate that all of the values of $\mathcal{C}_1$ for the $[(+45_2/0/90)_m]_s$ and $[(0/90/+45_2)_m]_s$ laminates are less than approximately 0.1. These values indicate that the contribution of $\mathcal{C}_1$ to the anisotropy factor defined by Eq. (33) is practically negligible. Thus, $\mathcal{A} \approx \mathcal{A}_0$ for these laminates. The values of $\mathcal{A}_0$ shown in Fig. 11 suggest that neglecting the anisotropy would, at most, underestimate the bending boundary-layer decay length by approximately a 10%. The insignificance of $\mathcal{C}_1$ also means that the coupling of the membrane and flexural anisotropies are unimportant with regards to the primary effect of the individual shell anisotropies that is captured by the parameter $\mathcal{A}_0$.

Balanced, Unsymmetrically Laminated Cylinders

Balanced, unsymmetric laminates may, in general, exhibit anisotropy in the form of coupling between pure bending and twisting ($D_{16} \neq D_{26} \neq 0$) and coupling between membrane and bending action, which is manifested by nonzero values for any of the subscripted B-terms in Eq. (A15). These laminates do not, however, exhibit extensional-shear coupling ($A_{16} = A_{26} = 0$). For the unsymmetric laminates that are discussed subsequently, the first ply in the stacking sequence is the innermost ply of a cylinder. Simplifed expressions for the anisotropy parameter $\mathcal{A}_0$ and the first-order correction factor $\mathcal{C}_1$, defined by Eqs. (33) - (35), are given by Eqs. (C27) and (C29), respectively. Equations (C28) and (C29) indicate that the value $\mathcal{C}_1$ depends on coupling between the flexural anisotropy and the anisotropy caused by unsymmetric lamination.

Results for regular, antisymmetric angle-ply laminates are shown in Figs. 4 and 12-16. In particular, values of the orthotropy parameter $\mathcal{O}$ for $[(\pm\phi)_m]_T$ unsymmetric laminates made of the nine material systems considered herein are also presented in Fig. 4; that is, the orthotropy-parameter curves presented in Fig. 4 for the $[(\pm\phi)_m]_s$ symmetric angle-ply laminates are also identical to those for $[(\pm\phi)_m]_T$ unsymmetric laminates. Thus, the orthotropy behavioral trends for the $[(\pm\phi)_m]_T$ unsymmetric laminates are identical to those discussed previously for the corresponding symmetric angle-ply laminates, and are also independent of the stacking sequence number m.

Results for the anisotropy parameter $\mathcal{A}_0$ defined by Eq. (C27) are shown in Fig. 12 for 2-ply $[\pm\phi]_T$ unsymmetric laminates made of the nine material systems considered herein. The results in Fig. 12 show a substantial variation in $\mathcal{A}_0$ with fiber orientation and with material system, and show that $\mathcal{A}_0$ is the most pronounced for values of the fiber angle ϕ between approximately 15 deg and 60 deg. Moreover, the largest variation in $\mathcal{A}_0$ with fiber angle is exhibited by the laminates made of the P-100/3502 pitch-epoxy material and the smallest variation is exhibited by the laminates made of boron-aluminum material. Values of $\mathcal{A}_0$ range from approximately 0.75 for the minimum point on the curve for the P-100/3502 pitch-epoxy material to a value of 1. The results in Fig. 13 show the variation in $\mathcal{A}_0$ with the fiber angle ϕ and the stacking sequence number m for $[(\pm\phi)_m]_T$ unsym-

metric laminates made of the P-100/3502 pitch-epoxy material. These results show a rapid decline in the importance of $\mathcal{A}_0$, that is manifested by the curve moving closer to $\mathcal{A}_0 = 1$, as the stacking sequence number increases. For m = 2, $0.95 < \mathcal{A}_0 < 1$.

Results for the first-order correction factor $\mathcal{C}_1$ are shown in Fig. 14 for 2-ply $[\pm\phi]_T$ unsymmetric laminates made of the nine material systems considered herein. The results in Fig. 14 also show a substantial variation in $\mathcal{C}_1$ with fiber orientation and with material system. However, the maximum magnitude of $\mathcal{C}_1$ is less than 0.07 for all of the material systems. Results are presented in Fig. 15 that show the variation in $\mathcal{C}_1$ with the fiber angle ϕ and the stacking sequence number m for $[(\pm\phi)_m]_T$ unsymmetric laminates made of the P-100/3502 pitch-epoxy material. These results show significant reductions in $\mathcal{C}_1$ with an increase in the stacking sequence number.

Overall, the results in Figs. 14 and 15 indicate that the contribution of $\mathcal{C}_1$ to the anisotropy factor defined by Eq. (33) is negligible for the upper bound of thinness given by h/R = 1/20, which means that $\mathcal{A} \approx \mathcal{A}_0$. Thus, the results in Fig. 12 for the two-ply $[\pm\phi]_T$ unsymmetric laminates indicate that neglecting the shell anisotropy overestimates the bending boundary layer, by as much as approximately 33% and 22% for shell walls made of P-100/3502 pitch-epoxy and IM7/5260 graphite-bismaleimide materials, respectively. The insignificance of $\mathcal{C}_1$ also means that the coupling of the flexural anisotropy and the anisotropy caused by unsymmetric lamination is unimportant with regards to the primary effect of the individual shell anisotropies. The insignificance of $\mathcal{C}_1$ is illustrated in Fig. 16 by the gray and by the black curves for the laminates made of P-100/3502 pitch-epoxy and IM7/5260 graphite-bismaleimide materials, respectively. The solid black and gray curves are for the upper bound of thin-shell theory that is given by h/R = 1/20. The finely dashed curves shown in the Fig. 16 correspond to 90%-decay lengths for which the anisotropy is neglected. In contrast, the solid curves include the effect of the shell anisotropy and are shown for values of $\mu = 0$, 1, and 1.5. The solid curves for $\mu = 1$ and 1.5 are based on the exact solution that uses Eq. (20b). The corresponding curves that are based on the approximate formula for the anisotropy parameter that is given by Eq. (33) are identical. The solid curves indicate no significant effect of varying μ, which implies that all three shell theories yield essentially the same results for the $[\pm\phi]_T$ unsymmetric laminates. For $[(\pm\phi)_m]_T$ unsymmetric laminates with m > 1 and made from any of the nine material systems considered herein, the results in Figs. 12 through 15 indicate that neglecting the shell-wall anisotropy will have a small effect on the calculation of the bending boundary-layer decay length.

Values of the orthotropy parameter $\mathcal{O}$ and the anisotropy parameter $\mathcal{A}_0$ for $(0_p/90_q)_T$ unsymmetric cross-ply laminates are shown in Figs. 17 and 18 for the nine material systems considered herein and as a function of the percentage of zero-degree plies. For this class of laminates, Eq. (20b) simplifies to Eq. (34); that is, $\mathcal{A} = \mathcal{A}_0$. This simplification means that the anisotropy parameter is independent of μ, which means that all three of the shell theories considered herein yield identical results.

The results in Fig. 17 show a large variation in $\mathcal{O}$ with the percentage of zero-deg plies for most of the material systems. In addition, the results show a large variation in $\mathcal{O}$ with material system for the laminates that are dominated by ninety-deg plies (less than approximately 10% zero-deg plies) and by zero-deg plies (more than approximately 80% zero-deg plies). Values of $\mathcal{O}$ vary the most for laminates made of P-100/3502 pitch-epoxy material, with values that range from approximately 0.3 to 2.93. Most of the materials exhibit values of $\mathcal{O}$ in the range of approximately 0.5 to 2.1.

The results in Fig. 18 also show a large variation in $\mathcal{A}_0$ with the percentage of zero-deg plies for most of the material systems, and show a large variation with material system for laminates with less than 70% zero-deg plies. Moreover, the results show that $\mathcal{A}_0$ is the most pronounced (most different from a value of 1) for laminates with approximately 15% to 30% zero-deg plies. The largest variation in $\mathcal{A}_0$ with percentage of zero-deg plies is exhibited by the laminates made of the P-100/3502 pitch-epoxy material and the smallest variation is exhibited by the laminates made of boron-aluminum material. Values of $\mathcal{A}_0$ range from approximately 0.57 for the minimum point on the curve for the P-100/3502 pitch-epoxy material to a value of 1. Thus, in some cases neglecting the shell wall anisotropy overestimates the bending boundary layer, by as much as approximately 75% for a shell wall made of P-100/3502 pitch-epoxy material. This result is illustrated in Fig. 19 by the gray curves. Similar results are presented in Fig. 19 for $(0_p/90_q)_T$ unsymmetric cross-ply laminates made of IM7/5260 graphite-bismaleimide material (black curves). The solid black and gray curves include the effect of the shell anisotropy and the finely dashed curves shown in the figure correspond to 90%-decay lengths for which the anisotropy is neglected. The results in Fig. 19 show that including the effect of anisotropy is particularly important for laminates with less than approximately 70% zero-deg plies.

Unbalanced, Unsymmetrically Laminated Cylinders

Unbalanced, unsymmetric laminates may, in gen-

eral, exhibit full anisotropy in the form of coupling between pure bending and twisting ($D_{16} \neq D_{26} \neq 0$) and coupling between membrane and bending action, which is manifested by nonzero values for any of the subscripted B-terms in Eq. (A15), and extensional-shear coupling ($A_{16} \neq A_{26} \neq 0$). The expressions for the anisotropy parameter $\mathcal{A}_0$ and the first-order correction factor $\mathcal{C}_1$ that are given by Eqs. (C2) - (C22) indicate that $\mathcal{A}_0$ exhibits coupling between the membrane anisotropy and the anisotropy that is caused by unsymmetric lamination, and that $\mathcal{C}_1$ exhibits coupling between all three types of anisotropies. One family of laminates that exhibits all of these anisotropies is the $(70_p/0_q)_T$ unbalanced, unsymmetric laminates with $p > 0$ and $q \neq 0$.

Values of the orthotropy parameter $\mathcal{O}$ and the anisotropy parameter $\mathcal{A}_0$ for $(70_p/0_q)_T$ unbalanced, unsymmetric laminates are shown in Figs. 20 and 21, respectively, for the nine material systems considered herein and as a function of the percentage of seventy-deg plies. The results in Fig. 20 show a large variation in $\mathcal{O}$ with the percentage of seventy-deg plies for most of the material systems. The results also show a large variation in $\mathcal{O}$ with material system for the laminates that are dominated by zero-deg plies (less than approximately 20% seventy-deg plies). Values of $\mathcal{O}$ vary the most for the laminates made of P-100/3502 pitch-epoxy material, with values that range from approximately 0.5 to 3.

The results in Fig. 21 also show a substantial variation in $\mathcal{A}_0$ with the percentage of seventy-deg plies for most of the material systems, and a large variation with material system for laminates with between approximately 45% and 100% seventy-deg plies. The largest overall variation in $\mathcal{A}_0$ with percentage of seventy-deg plies is exhibited by the laminates made of the P-100/3502 pitch-epoxy material and the smallest variation is exhibited by the laminates made of boron-aluminum material. Values of $\mathcal{A}_0$ range from approximately 1.4 to 0.95, which correspond to the maximum and minimum points, respectively, on the curve for the P-100/3502 pitch-epoxy material.

Results for the first-order correction factor $\mathcal{C}_1$ were also obtained for $(70_p/0_q)_T$ unbalanced, unsymmetric laminates made of the nine material systems considered herein, but are not included in the present paper. These results also show a substantial, relative variation in $\mathcal{C}_1$ with the percentage of seventy-deg plies, but overall the magnitude of $\mathcal{C}_1$ is less than approximately 0.25 for the P-100/3502 pitch-epoxy material and less than 0.1 for the other materials. These results indicate that the contribution of $\mathcal{C}_1$ to the anisotropy factor defined by Eq. (33) is negligible for the upper bound of thin-shell theory that is given by h/R = 1/20, which means that $\mathcal{A} \approx \mathcal{A}_0$. Thus, the results in Fig. 21 suggest that in some cases neglecting the shell-wall anisotropy may overestimate the bending boundary-layer decay length and in other cases, may underestimate the decay length. The insignificance of $\mathcal{C}_1$ also means that the contribution of the flexural anisotropy to the coupling of the anisotropies is negligible. The insignificance of $\mathcal{C}_1$ is clarified in Fig. 22 for laminates made of P-100/3502 pitch-epoxy material (gray curves) and of IM7/5260 graphite-bismaleimide material (black curves). The solid black and gray curves are for the upper bound of thinness given by h/R = 1/20. The finely dashed curves shown in the figure correspond to 90%-decay lengths for which the anisotropy is neglected. In contrast, the solid curves include the effect of the shell anisotropy and are shown for values of $\mu = 0$, 1, and 1.5. Moreover, the solid curves for $\mu = 1$ and 1.5 are based on the exact solution that uses Eq. (20b). The corresponding curves that are based on the approximate formula for the anisotropy parameter that is given by Eq. (33) are identical. The solid curves indicate a negligible effect of varying μ, which verifies that $\mathcal{A} \approx \mathcal{A}_0$ and implies that all three shell theories yield essentially the same results for the $(70_p/0_q)_T$ unbalanced, unsymmetric laminates. In addition, the results show that neglecting the shell wall anisotropy, for the most part, underestimates the bending boundary-layer decay length, by as much as approximately 16% and 6% for shell walls made of P-100/3502 pitch-epoxy and IM7/5260 graphite-bismaleimide materials, respectively, and with approximately 20% seventy-deg plies. In addition, the results in Fig. 22 show that neglecting the shell wall anisotropy underestimates the bending boundary-layer decay length, by as much as approximately 31% and 20% for shell walls made of P-100/3502 pitch-epoxy and IM7/5260 graphite-bismaleimide materials, respectively, and with approximately 100% seventy-deg plies. There is only a very small range shown in Fig. 22 where neglecting the shell wall anisotropy overestimates the bending boundary-layer decay length, and for this region, the effect is negligible.

Concluding Remarks

An analytical study of the attenuation of bending boundary layers in both balanced and unbalanced, symmetrically and unsymmetrically laminated-composite, thin cylindrical shells has been presented for nine contemporary material systems. The analysis is based on the linear Sanders-Koiter shell equations and contains the Love-Kirchhoff shell equations and Donnell's equations as special cases. With this analysis, two nondimensional parameters have been indentified that characterize and quantify the effects of laminate orthotropy and laminate

anisotropy on the bending boundary-layer decay length in a very general and encompassing manner. The anisotropy parameter includes the effects of anisotropy in the form of coupling between pure bending and twisting that appears in many symmetric laminates to some extent, coupling between extension and shear that is present in unbalanced laminates, and coupling between membrane and bending action that is present in unsymmetric laminates.

A substantial number of structural design technology results for the bending boundary-layer decay length have been presented for a wide range of laminated-composite shell structures that should be useful additions to the structural designer's collection of preliminary design tools. Moreover, the analysis and results should provide additional physical insight into the fundamental behavior of general laminated composite shell structures and provide a common basis for assessing bending boundary-layer attenuation for the vast range of laminate constructions that are possible. Furthermore, the results should be useful for the design of specimens for material characterization tests, for instrumenting structural verification tests, and for defining finite-element meshes. For all the laminate constructions considered in the present study, the results show that the differences between results that were obtained with the Sanders-Koiter shell equations, the Love-Kirchhoff shell equations, and Donnell's equations are negligible. The results also show that the effect of anisotropy in the form of coupling between pure bending and twisting has a neglible effect on the size of the bending boundary-layer attenuation length of the balanced, symmetrically laminated cylinders considered. Moreover, the results show that the coupling of the membrane and flexural anisotropy and the anisotropy caused by unsymmetric lamination is generally unimportant with regards to the primary effect of the individual shell anisotropies on the bending boundary-layer decay length. The only exception encountered was for unbalanced, unsymmetrically laminated cylinders for which coupling of the membrane anisotropy and the anisotropy caused by unsymmetric lamination is a primary effect, as expected. The results also show that in some cases neglecting the shell anisotropy results in underestimating the bending boundary-layer decay length and in other cases it results in an overestimation.

Appendix A: Sanders-Koiter Equations

The linear Sanders-Koiter shell equations[16,17] are presented in this appendix for a right-circular cylinder with a radius that is given by R. For these equations, x and θ denote the axial and circumferential coordinates, respectively. First, the equilibrium equations are presented, then the kinematic equations and the constitutive equations are presented. Last, the boundary conditions are given for a complete right-circular cylinder at an edge that is given by a constant value of the axial coordinate, x.

Equilibrium Equations

The equilibrium equations are given in a form similar to those found in Ref. 22; that is,

$$\frac{\partial N_x}{\partial x} + \frac{1}{R}\frac{\partial N_{x\theta}}{\partial \theta} - \frac{c_2}{2R^2}\frac{\partial M_{x\theta}}{\partial \theta} + q_x = 0 \qquad \text{(A1)}$$

$$\frac{\partial N_{x\theta}}{\partial x} + \frac{1}{R}\frac{\partial N_\theta}{\partial \theta} + \frac{c_1}{R}Q_\theta + \frac{c_2}{2R}\frac{\partial M_{x\theta}}{\partial x} + q_\theta = 0 \qquad \text{(A2)}$$

$$\frac{\partial Q_x}{\partial x} + \frac{1}{R}\frac{\partial Q_\theta}{\partial \theta} - \frac{N_\theta}{R} + q_n = 0 \qquad \text{(A3)}$$

$$\frac{\partial M_x}{\partial x} + \frac{1}{R}\frac{\partial M_{x\theta}}{\partial \theta} - Q_x = 0 \qquad \text{(A4)}$$

$$\frac{\partial M_{x\theta}}{\partial x} + \frac{1}{R}\frac{\partial M_\theta}{\partial \theta} - Q_\theta = 0 \qquad \text{(A5)}$$

where N_x, N_θ, and $N_{x\theta}$ are the membrane stress resultants; Q_x and Q_θ are the transverse shear-stress resultants; M_x, M_θ, and $M_{x\theta}$ are the bending stress resultants; q_x, q_θ, and q_n are the applied surface tractions; and c_1 and c_2 are constants that identify the equations of other shell theories that are considered herein. In particular, the Sanders-Koiter equations are given by $c_1 = c_2 = 1$ and the Love-Kirchhoff equations are give by $c_1 = 1$ and $c_2 = 0$. Donnell's equations are given by $c_1 = c_2 = 0$. This convention is used throughout the present study.

Kinematic Equations

The kinematic equations are given by

$$\varepsilon_x^o = \frac{\partial u}{\partial x} \qquad \text{(A6)}$$

$$\varepsilon_\theta^n = \frac{1}{R}\frac{\partial v}{\partial \theta} + \frac{w}{R} \qquad \text{(A7)}$$

$$\gamma_{x\theta}^n = \frac{\partial v}{\partial x} + \frac{1}{R}\frac{\partial u}{\partial \theta} \qquad \text{(A8)}$$

$$\beta_x^o = -\frac{\partial w}{\partial x} \qquad \text{(A9)}$$

$$\beta_\theta^o = \frac{c_1}{R}v - \frac{1}{R}\frac{\partial w}{\partial \theta} \qquad \text{(A10)}$$

$$\beta_n^o = \frac{c_2}{2}\left(\frac{\partial v}{\partial x} - \frac{1}{R}\frac{\partial u}{\partial \theta}\right) \qquad \text{(A11)}$$

$$\kappa_x^o = \frac{\partial \beta_x^o}{\partial x} = -\frac{\partial^2 w}{\partial x^2} \tag{A12}$$

$$\kappa_\theta^o = \frac{1}{R}\frac{\partial \beta_\theta^o}{\partial \theta} = \frac{c_1}{R^2}\frac{\partial v}{\partial \theta} - \frac{1}{R^2}\frac{\partial^2 w}{\partial \theta^2} \tag{A13}$$

$$\kappa_{x\theta}^o = \frac{1}{R}\left(\frac{\partial \beta_x^o}{\partial \theta} + \beta_n^o\right) + \frac{\partial \beta_\theta^o}{\partial x}$$
$$= -\frac{2}{R}\frac{\partial^2 w}{\partial x \partial \theta} + \frac{1}{R}\left(c_1 + \frac{1}{2}c_2\right)\frac{\partial v}{\partial x} - \frac{c_2}{2R^2}\frac{\partial u}{\partial \theta} \tag{A14}$$

where u, v, and w are the axial, circumferential, and normal displacements of a point of the shell middle surface; ε_x^o, ε_θ^o, and $\gamma_{x\theta}^o$ are the membrane strains; β_x^o, β_θ^o, and β_n^o are the rotations; and κ_x^o, κ_θ^o, and $\kappa_{x\theta}^o$ are the bending strains. The displacement w is positive when it is outward from the cylinder reference surface.

Constitutive Equations

The isothermal constitutive equations are given in matrix form by

$$\begin{Bmatrix} N_x \\ N_\theta \\ N_{x\theta} \\ \hline M_x \\ M_\theta \\ M_{x\theta} \end{Bmatrix} = \left[\begin{array}{ccc:ccc} A_{11} & A_{12} & A_{16} & B_{11} & B_{12} & B_{16} \\ A_{12} & A_{22} & A_{26} & B_{12} & B_{22} & B_{26} \\ A_{16} & A_{26} & A_{66} & B_{16} & B_{26} & B_{66} \\ \hdashline B_{11} & B_{12} & B_{16} & D_{11} & D_{12} & D_{16} \\ B_{12} & B_{22} & B_{26} & D_{12} & D_{22} & D_{26} \\ B_{16} & B_{26} & B_{66} & D_{16} & D_{26} & D_{66} \end{array}\right] \begin{Bmatrix} \varepsilon_x^o \\ \varepsilon_\theta^o \\ \gamma_{x\theta}^o \\ \hline \kappa_x^o \\ \kappa_\theta^o \\ \kappa_{x\theta}^o \end{Bmatrix} \tag{A15}$$

where the subscripted A, B, and D terms of the matrix are the stiffnesses of laminated composite shells that are obtained from the Love-Kirchhoff shell theory. Moreover, the constitutive terms in Eq. (A15) are identical to those for laminated-composite plates that are given in Ref. 18, p. 198.

Boundary Conditions

The boundary conditions for an edge that is defined by a constant value of the axial coordinate x are given by

$$N_x = \bar{N}_x(\theta) \quad \text{or} \quad u = \bar{u}(\theta) \tag{A16}$$

$$N_{x\theta} + \frac{1}{R}\left(c_1 + \frac{1}{2}c_2\right)M_{x\theta} = \bar{T}(\theta) \quad \text{or} \quad v = \bar{v}(\theta) \tag{A17}$$

$$Q_x + \frac{1}{R}\frac{\partial M_{x\theta}}{\partial \theta} = \bar{V}(\theta) \quad \text{or} \quad w = \bar{w}(\theta) \tag{A18}$$

$$M_x = \bar{M}_x(\theta) \quad \text{or} \quad \beta_x^o = \bar{\beta}(\theta) \tag{A19}$$

where $\bar{u}(\theta)$, $\bar{v}(\theta)$, and $\bar{w}(\theta)$ are applied edge displacements; $\bar{\beta}(\theta)$ is an applied edge rotation; and $\bar{N}_x(\theta)$, $\bar{T}(\theta)$, $\bar{V}(\theta)$, and $\bar{M}_x(\theta)$ are applied edge loads.

Appendix B: Equations for Axisymmetry

The linear Sanders-Koiter shell equations that are presented in Appendix A for a right-circular cylinder with a radius R are specialized in this appendix for the case of axisymmetric behavior. For these equations, x and θ denote the axial and circumferential coordinates, respectively. The specialization to axial symmetry is conducted by eliminating all terms in the equations of Appendix A that are differentiatied with respect to the circumferential coordinate, θ. First, the equilibrium equations, the kinematic equations, and the constitutive equations are presented. Then, the boundary conditions are given for a complete right-circular cylinder at an edge that is given by a constant value of the axial coordinate, x. Last, the axisymmetric equations are manipulated into a single ordinary differential equation in terms of the normal displacement w(x).

Equilibrium Equations

The equilibrium equations for axisymmetric behavior are given by

$$\frac{dN_x}{dx} + q_x(x) = 0 \tag{B1}$$

$$\frac{dN_{x\theta}}{dx} + \frac{c_1}{R}Q_\theta + \frac{c_2}{2R}\frac{dM_{x\theta}}{dx} + q_\theta(x) = 0 \tag{B2}$$

$$\frac{dQ_x}{dx} - \frac{N_\theta}{R} + q_n(x) = 0 \tag{B3}$$

$$\frac{dM_x}{dx} - Q_x = 0 \tag{B4}$$

$$\frac{dM_{x\theta}}{dx} - Q_\theta = 0 \tag{B5}$$

where the membrane stress resultants N_x, N_θ, and $N_{x\theta}$; the transverse shear-stress resultants Q_x and Q_θ; the bending stress resultants M_x, M_θ, and $M_{x\theta}$; and the applied surface tractions q_x, q_θ, and q_n are functions of only the axial coordinate, x.

Kinematic Equations

The kinematic equations are given by

$$\varepsilon_x^o = \frac{du}{dx} \tag{B6}$$

$$\varepsilon_\theta^o = \frac{w}{R} \tag{B7}$$

$$\gamma_{x\theta}^o = \frac{dv}{dx} \tag{B8}$$

$$\beta_x^o = -\frac{dw}{dx} \tag{B9}$$

$$\beta_\theta^o = \frac{c_1}{R} v \tag{B10}$$

$$\beta_n^o = \frac{c_2}{2}\frac{dv}{dx} \tag{B11}$$

$$\kappa_x^o = \frac{d\beta_x^o}{dx} = -\frac{d^2w}{dx^2} \tag{B12}$$

$$\kappa_\theta^o = 0 \tag{B13}$$

$$\kappa_{x\theta}^o = \frac{1}{R}\beta_n^o + \frac{d\beta_\theta^o}{dx} = \frac{1}{R}\left(c_1 + \frac{1}{2}c_2\right)\frac{dv}{dx} \tag{B14}$$

where the middle-surface displacements u, v, and w; the membrane strains ε_x^o, ε_θ^o, and $\gamma_{x\theta}^o$; the rotations β_x^o, β_θ^o, and β_n^o; and the bending strains κ_x^o and $\kappa_{x\theta}^o$ are functions of only the axial coordinate, x.

Constitutive Equations

The isothermal constitutive equations reduce to

$$\begin{Bmatrix} N_x \\ N_\theta \\ N_{x\theta} \\ M_x \\ M_\theta \\ M_{x\theta} \end{Bmatrix} = \left[\begin{array}{ccc:ccc} A_{11} & A_{12} & A_{16} & B_{11} & B_{12} & B_{16} \\ A_{12} & A_{22} & A_{26} & B_{12} & B_{22} & B_{26} \\ A_{16} & A_{26} & A_{66} & B_{16} & B_{26} & B_{66} \\ \hdashline B_{11} & B_{12} & B_{16} & D_{11} & D_{12} & D_{16} \\ B_{12} & B_{22} & B_{26} & D_{12} & D_{22} & D_{26} \\ B_{16} & B_{26} & B_{66} & D_{16} & D_{26} & D_{66} \end{array}\right] \begin{Bmatrix} \varepsilon_x^o \\ \varepsilon_\theta^o \\ \gamma_{x\theta}^o \\ \kappa_x^o \\ 0 \\ \kappa_{x\theta}^o \end{Bmatrix} \tag{B15}$$

where the subscripted A, B, and D terms of the matrix are the usual constitutive terms of classical Love-Kirchhoff-type laminated composite shell theory or classical laminated plate theory (e.g., see p. 198 of Ref. 18).

Boundary Conditions

The boundary conditions for an edge that is defined by a constant value of the axial coordinate x are given by

$$N_x = \bar{N}_x \quad \text{or} \quad u = \bar{u} \tag{B16}$$

$$N_{x\theta} + \frac{1}{R}\left(c_1 + \frac{1}{2}c_2\right)M_{x\theta} = \bar{T} \quad \text{or} \quad v = \bar{v} \tag{B17}$$

$$Q_x = \bar{V} \quad \text{or} \quad w = \bar{w} \tag{B18}$$

$$M_x = \bar{M}_x \quad \text{or} \quad \beta_x^o = \bar{\beta} \tag{B19}$$

where the applied edge displacements $\bar{u}$, $\bar{v}$, and $\bar{w}$; the applied edge rotation $\bar{\beta}$; and the applied edge loads $\bar{N}_x$, $\bar{T}$, $\bar{V}$, and $\bar{M}_x$ are all constants.

Bending Boundary-Layer Equation

The bending boundary-layer equation is obtained by first noting that integration of Eq. (B1) yields

$$N_x = -\int q_x\,dx + C \equiv \bar{N}(x) \tag{B20}$$

where C is a constant of integration that is determined from the boundary condition given by Eq. (B16). Next, Eqs. (B2) and (B5) are combined to get

$$\frac{dN_{x\theta}}{dx} + \frac{1}{R}\left(c_1 + \frac{1}{2}c_2\right)\frac{dM_{x\theta}}{dx} + q_\theta(x) = 0 \tag{B21}$$

For convenience, the parameter

$$\mu = c_1 + \frac{1}{2}c_2 \tag{B22}$$

is introduced such that the Sanders-Koiter equations are given by $\mu = \frac{3}{2}$ and the Love-Kirchhoff equations are given by $\mu = 1$. Donnell's equations are given by $\mu = 0$. Similarly, the function

$$\hat{T}(x) = N_{x\theta} + \frac{\mu}{R}M_{x\theta} \tag{B23}$$

is introduced so that Eq. (B21) becomes

$$\frac{d\hat{T}}{dx} + q_\theta(x) = 0 \tag{B24}$$

and the corresponding boundary condition given by Eq. (B17) becomes

$$\hat{T} = \bar{T} \quad \text{or} \quad v = \bar{v} \tag{B25}$$

Integration of Eq. (B24) yields

$$\hat{T} = -\int q_\theta\,dx + C \equiv \bar{T}(x) \tag{B26}$$

where C is a constant of integration that is determined from the boundary condition given by Eq. (B25). Next, Eqs. (B3) and (B4) are combined to give

$$\frac{d^2M_x}{dx^2} - \frac{N_\theta}{R} + q_n(x) = 0 \qquad \text{(B27)}$$

The next step in the analysis is the simplification of the constitutive equations. First, by using Eqs. (B8) and (B22), Eq. (B14) is expressed as

$$\kappa^o_{x\theta} = \frac{\mu}{R}\gamma^o_{x\theta} \qquad \text{(B28)}$$

By using Eqs. (B23) and (B28), the constitutive equations are expressed as

$$\begin{Bmatrix} N_x \\ N_\theta \\ \hat{T} \\ M_x \end{Bmatrix} = \begin{bmatrix} A_{11} & A_{12} & \bar{A}_{16} & B_{11} \\ A_{12} & A_{22} & \bar{A}_{26} & B_{12} \\ \bar{A}_{16} & \bar{A}_{26} & \bar{A}_{66} & \bar{B}_{16} \\ B_{11} & B_{12} & \bar{B}_{16} & D_{11} \end{bmatrix} \begin{Bmatrix} \varepsilon^o_x \\ \varepsilon^o_\theta \\ \gamma^o_{x\theta} \\ \kappa^o_x \end{Bmatrix} \qquad \text{(B29)}$$

and

$$M_\theta = B_{12}\varepsilon^o_x + B_{22}\varepsilon^o_\theta + \bar{B}_{26}\gamma^o_{x\theta} + D_{12}\kappa^o_x \qquad \text{(B30)}$$

where

$$\bar{A}_{16} = A_{16} + \mu\left(\frac{h}{R}\right)\frac{B_{16}}{h} \qquad \text{(B31)}$$

$$\bar{A}_{26} = A_{26} + \mu\left(\frac{h}{R}\right)\frac{B_{26}}{h} \qquad \text{(B32)}$$

$$\bar{A}_{66} = A_{66} + 2\mu\left(\frac{h}{R}\right)\frac{B_{66}}{h} + \mu^2\left(\frac{h}{R}\right)^2\frac{D_{66}}{h^2} \qquad \text{(B33)}$$

$$\bar{B}_{16} = B_{16} + \mu\left(\frac{h}{R}\right)\frac{D_{16}}{h} \qquad \text{(B34)}$$

$$\bar{B}_{26} = B_{26} + \mu\left(\frac{h}{R}\right)\frac{D_{26}}{h} \qquad \text{(B35)}$$

The motivation for writing the constitutive equations in this form is that the matrix equation given by Eq. (B29) is the only part of the of the full constitutive equations that appear in the strain energy density function, which is used in the present paper to determine the corresponding positive-definiteness conditions. With these simplified constitutive equations and Eqs. (B6) - (B8) and (B12), Eq. (B20) is expressed as

$$A_{11}\frac{du}{dx} + A_{12}\frac{w}{R} + \bar{A}_{16}\frac{dv}{dx} - B_{11}\frac{d^2w}{dx^2} - \bar{N}(x) = 0 \qquad \text{(B36)}$$

and Eq. (B26) is expressed as

$$\bar{A}_{16}\frac{du}{dx} + \bar{A}_{26}\frac{w}{R} + \bar{A}_{66}\frac{dv}{dx} - \bar{B}_{16}\frac{d^2w}{dx^2} - \bar{T}(x) = 0 \qquad \text{(B37)}$$

Equations (B36) and (B37) are then solved for $\frac{du}{dx}$ and $\frac{dv}{dx}$ to get

$$\frac{du}{dx} = \frac{\bar{A}_{66}\bar{N}(x) - \bar{A}_{16}\bar{T}(x)}{A_{11}\bar{A}_{66} - \bar{A}_{16}^2} + \frac{\left(\bar{A}_{16}\bar{A}_{26} - A_{12}\bar{A}_{66}\right)\frac{w}{R} + \left(\bar{A}_{66}B_{11} - \bar{A}_{16}\bar{B}_{16}\right)\frac{d^2w}{dx^2}}{A_{11}\bar{A}_{66} - \bar{A}_{16}^2} \qquad \text{(B38)}$$

$$\frac{dv}{dx} = \frac{A_{11}\bar{T}(x) - \bar{A}_{16}\bar{N}(x)}{A_{11}\bar{A}_{66} - \bar{A}_{16}^2} + \frac{\left(A_{12}\bar{A}_{16} - A_{11}\bar{A}_{26}\right)\frac{w}{R} + \left(A_{11}\bar{B}_{16} - \bar{A}_{16}B_{11}\right)\frac{d^2w}{dx^2}}{A_{11}\bar{A}_{66} - \bar{A}_{16}^2} \qquad \text{(B39)}$$

Equation (B39) indicates that the circumferential displacement v(x) becomes uncoupled from the axial displacement u(x) and the normal displacement w(x) when $\bar{A}_{16} = \bar{A}_{26} = \bar{B}_{16} = 0$, which implies that $A_{16} = A_{26} = B_{16} = B_{26} = D_{16} = 0$. In addition, the constitutive equation, Eq. (B29), indicates that N_x, N_θ, and M_x become uncoupled from the torsional, shear strain $\gamma^o_{x\theta}$ when $\bar{A}_{16} = \bar{A}_{26} = \bar{B}_{16} = 0$, and that $\hat{T}$, that is defined by Eq. (B23), becomes uncoupled from ε^o_x, ε^o_θ, and κ^o_x. Furthermore, Eq. (B30) indicates that M_θ becomes uncoupled from $\gamma^o_{x\theta}$ when $\bar{B}_{26} = 0$, which implies $B_{26} = D_{26} = 0$.

Next, Eqs. (B38) and (B39) are then substituted into Eqs. (B6) and (B8), and the resulting expressions for ε^o_x and $\gamma^o_{x\theta}$, along with Eqs. (B7) and (B12) are substituted into the constitutive equations, (B29). This action converts the strains and stress resultants in Eq. (B29) into functions of the displacement w(x). Substituting the expressions for N_θ and M_x into Eq. (B27) yields the bending boundary-layer equation that is given by

$$C_1\frac{d^4w}{dx^4} + C_2\frac{d^2w}{dx^2} + C_3w = C_4(x) \qquad \text{(B40)}$$

The constant coefficients are given by

$$C_1 = D_{11}\left(1 - \frac{\bar{A}_{66}B_{11}^2 + A_{11}\bar{B}_{16}^2 - 2\bar{A}_{16}B_{11}\bar{B}_{16}}{\left(A_{11}\bar{A}_{66} - \bar{A}_{16}^2\right)D_{11}}\right) \quad \text{(B41)}$$

$$C_2 = -\frac{2}{R}B_{12} - \frac{2}{R}\left(\frac{\left(\bar{A}_{16}\bar{A}_{26} - A_{12}\bar{A}_{66}\right)B_{11} + \left(A_{12}\bar{A}_{16} - A_{11}\bar{A}_{26}\right)\bar{B}_{16}}{A_{11}\bar{A}_{66} - \bar{A}_{16}^2}\right) \quad \text{(B42)}$$

$$C_3 = \frac{\left(A_{11}A_{22} - A_{12}^2\right)\bar{A}_{66} - A_{11}\bar{A}_{26}^2 - A_{22}\bar{A}_{16}^2 + 2A_{12}\bar{A}_{16}\bar{A}_{26}}{R^2\left(A_{11}\bar{A}_{66} - \bar{A}_{16}^2\right)} \quad \text{(B43)}$$

The function $C_4(x)$ is given by

$$C_4(x) = q_n(x) + \frac{\left(\bar{A}_{16}\bar{A}_{26} - A_{12}\bar{A}_{66}\right)\bar{N}(x) + \left(A_{12}\bar{A}_{16} - A_{11}\bar{A}_{26}\right)\bar{T}(x)}{R\left(A_{11}\bar{A}_{66} - \bar{A}_{16}^2\right)} + \frac{\left(B_{11}\bar{A}_{66} - \bar{A}_{16}\bar{B}_{16}\right)\frac{d^2\bar{N}}{dx^2} + \left(A_{11}\bar{B}_{16} - B_{11}\bar{A}_{16}\right)\frac{d^2\bar{T}}{dx^2}}{\left(A_{11}\bar{A}_{66} - \bar{A}_{16}^2\right)} \quad \text{(B44)}$$

These expressions are simplifed further by introducing the following expressions

$$\bar{a}_{12} = \frac{\bar{A}_{16}\bar{A}_{26} - A_{12}\bar{A}_{66}}{\left(A_{11}A_{22} - A_{12}^2\right)\bar{A}_{66} - A_{11}\bar{A}_{26}^2 - A_{22}\bar{A}_{16}^2 + 2A_{12}\bar{A}_{16}\bar{A}_{26}} \quad \text{(B45)}$$

$$\bar{a}_{22} = \frac{A_{11}\bar{A}_{66} - \bar{A}_{16}^2}{\left(A_{11}A_{22} - A_{12}^2\right)\bar{A}_{66} - A_{11}\bar{A}_{26}^2 - A_{22}\bar{A}_{16}^2 + 2A_{12}\bar{A}_{16}\bar{A}_{26}} \quad \text{(B46)}$$

$$\bar{a}_{26} = \frac{A_{12}\bar{A}_{16} - A_{11}\bar{A}_{26}}{\left(A_{11}A_{22} - A_{12}^2\right)\bar{A}_{66} - A_{11}\bar{A}_{26}^2 - A_{22}\bar{A}_{16}^2 + 2A_{12}\bar{A}_{16}\bar{A}_{26}} \quad \text{(B47)}$$

$$\bar{b}_{21} = -\left(\bar{a}_{12}B_{11} + \bar{a}_{22}B_{12} + \bar{a}_{26}\bar{B}_{16}\right) \quad \text{(B48)}$$

$$e = 1 - \frac{\bar{A}_{66}B_{11}^2 + A_{11}\bar{B}_{16}^2 - 2\bar{A}_{16}B_{11}\bar{B}_{16}}{\left(A_{11}\bar{A}_{66} - \bar{A}_{16}^2\right)D_{11}} \quad \text{(B49)}$$

By using Eqs. (B45) - (B49), Eqs. (B41) - (B43) are expressed as

$$C_1 = D_{11}e \quad \text{(B50)}$$

$$C_2 = \frac{2}{R}\frac{\bar{b}_{21}}{\bar{a}_{22}} \quad \text{(B51)}$$

$$C_3 = \frac{1}{R^2\bar{a}_{22}} \quad \text{(B52)}$$

Similarly, for the case where the second derivatives of $\bar{N}(x)$ and $\bar{T}(x)$ are zero valued, Eq. (B44) becomes

$$C_4(x) = q_n(x) + \frac{\bar{a}_{12}\bar{N}(x) + \bar{a}_{26}\bar{T}(x)}{R\bar{a}_{22}} \quad \text{(B53)}$$

The desired form of the bending boundary-layer equation is obtained by dividing Eq. (B40) by C_1; that is,

$$\frac{d^4w}{dx^4} + 4S\frac{d^2w}{dx^2} + 4Qw = P(x) \quad \text{(B54)}$$

where the constants S and Q are given by

$$S = \frac{C_2}{4C_1} = \frac{\bar{b}_{21}}{2R\bar{a}_{22}D_{11}e} \quad \text{(B55)}$$

$$Q = \frac{C_3}{4C_1} = \frac{1}{4R^2\bar{a}_{22}D_{11}e} \quad \text{(B56)}$$

The function P(x) is given by

$$P(x) = \frac{C_4(x)}{C_1} = \frac{q_n(x)}{D_{11}e} + \frac{\bar{a}_{12}\bar{N}(x) + \bar{a}_{26}\bar{T}(x)}{R\bar{a}_{22}D_{11}e} \quad \text{(B57)}$$

for the special case when the second derivatives of $\bar{N}(x)$ and $\bar{T}(x)$ are zero valued. The quantity $D_{11}e$ that appears in Eqs. (B54) - (B56) is sometimes referred to, in some contexts, as a reduced bending stiffness.[12]

Appendix C: Anisotropy-Factor Equations

The first-order approximation of the anisotropy factor $\mathcal{A}$ that is used herein is given by

$$\mathcal{A} \approx \mathcal{A}_0\left[1 + \mu\,\mathcal{C}_1\left(\frac{h}{R}\right)\right] \quad \text{(C1)}$$

where $\mathcal{A}_0$ is the value of Eq. (20b) with $\mu = 0$ in the terms with the overbars. This expression is given by

$$\mathcal{A}_0 = \left[\frac{\left(A_{11}A_{22} - A_{12}^2\right)}{A_{11}}a_{22}e_0\right]^{1/4}\left[1 - \frac{b_{21}}{\sqrt{a_{22}D_{11}e_0}}\right]^{-1/2} \quad \text{(C2)}$$

which is the anisotropy factor that corresponds to Donnell's equations. The terms a_{22}, b_{21}, and e_0 are given by

$$a_{12} = \frac{A_{16}A_{26} - A_{12}A_{66}}{\left(A_{11}A_{22} - A_{12}^2\right)A_{66} - A_{11}A_{26}^2 - A_{22}A_{16}^2 + 2A_{12}A_{16}A_{26}} \quad \text{(C3)}$$

$$a_{22} = \frac{A_{11}A_{66} - A_{16}^2}{\left(A_{11}A_{22} - A_{12}^2\right)A_{66} - A_{11}A_{26}^2 - A_{22}A_{16}^2 + 2A_{12}A_{16}A_{26}} \quad \text{(C4)}$$

$$a_{26} = \frac{A_{12}A_{16} - A_{11}A_{26}}{\left(A_{11}A_{22} - A_{12}^2\right)A_{66} - A_{11}A_{26}^2 - A_{22}A_{16}^2 + 2A_{12}A_{16}A_{26}} \quad \text{(C5)}$$

$$b_{21} = -\left(a_{12}B_{11} + a_{22}B_{12} + a_{26}B_{16}\right) \quad \text{(C6)}$$

$$e_0 = 1 - \frac{A_{66}B_{11}^2 + A_{11}B_{16}^2 - 2A_{16}B_{11}B_{16}}{\left(A_{11}A_{66} - A_{16}^2\right)D_{11}} \quad \text{(C7)}$$

The term $\mathcal{C}_1$ is a first-order correction to the results that correspond to Donnell's equations and is given by

$$\mathcal{C}_1 = \frac{\sqrt{a_{22}D_{11}e_0}\left(a_{22}e_1 + a_{122}e_0\right) + 2a_{22}\left(b_{121}e_0 - b_{21}e_1\right) - 2a_{122}b_{21}e_0}{4a_{22}e_0\left[\sqrt{a_{22}D_{11}e_0} - b_{21}\right]} \quad \text{(C8)}$$

where

$$e_1 = \frac{2\left(A_{16}B_{11} - A_{11}B_{16}\right)}{\left(A_{11}A_{66} - A_{16}^2\right)^2 D_{11}h}\Big[D_{16}\left(A_{11}A_{66} - A_{16}^2\right) + - B_{16}\left(B_{11}A_{66} + A_{11}B_{66}\right) + A_{16}\left(A_{11}B_{66} + B_{16}^2\right)\Big] \quad \text{(C9)}$$

$$a_{112} = \frac{B_{16}f_{16} + B_{26}f_{26} + B_{66}f_{66}}{\left[\left(A_{11}A_{22} - A_{12}^2\right)A_{66} - A_{11}A_{26}^2 - A_{22}A_{16}^2 + 2A_{12}A_{16}A_{26}\right]^2 h} \quad \text{(C10)}$$

$$a_{122} = -2\,\frac{B_{16}g_{16} + B_{26}g_{26} + B_{66}g_{66}}{\left[\left(A_{11}A_{22} - A_{12}^2\right)A_{66} - A_{11}A_{26}^2 - A_{22}A_{16}^2 + 2A_{12}A_{16}A_{26}\right]^2 h} \quad \text{(C11)}$$

$$a_{126} = \frac{B_{16}h_{16} + B_{26}h_{26} + B_{66}h_{66}}{\left[\left(A_{11}A_{22} - A_{12}^2\right)A_{66} - A_{11}A_{26}^2 - A_{22}A_{16}^2 + 2A_{12}A_{16}A_{26}\right]^2 h} \quad \text{(C12)}$$

$$b_{121} = -\left(a_{112}B_{11} + a_{122}B_{12} + a_{126}B_{16} + \frac{a_{26}D_{16}}{h}\right) \quad \text{(C13)}$$

and

$$f_{16} = A_{26}\left(A_{16}^2A_{22} - A_{11}A_{26}^2\right) + A_{66}\left[A_{26}\left(A_{11}A_{22} + A_{12}^2\right) - 2A_{12}A_{22}A_{16}\right] \quad \text{(C14)}$$

$$f_{26} = A_{16}\left(A_{26}^2A_{11} - A_{22}A_{16}^2\right) + A_{66}\left[A_{16}\left(A_{11}A_{22} + A_{12}^2\right) - 2A_{11}A_{12}A_{26}\right] \quad \text{(C15)}$$

$$f_{66} = 2\left(A_{12}A_{16} - A_{11}A_{26}\right)\left(A_{16}A_{22} - A_{12}A_{26}\right) \quad \text{(C16)}$$

$$g_{16} = \left(A_{12}A_{16} - A_{11}A_{26}\right)\left(A_{16}A_{26} - A_{12}A_{66}\right) \quad \text{(C17)}$$

$$g_{26} = \left(A_{12}A_{16} - A_{11}A_{26}\right)\left(A_{11}A_{66} - A_{16}^2\right) \quad \text{(C18)}$$

$$g_{66} = \left(A_{12}A_{16} - A_{11}A_{26}\right)^2 \quad \text{(C19)}$$

$$h_{16} = A_{12}A_{66}\left(A_{12}A_{66} - A_{12}^2\right) + A_{11}A_{26}\left(A_{12}A_{26} - A_{16}A_{22}\right) + A_{16}A_{22}\left(A_{12}A_{16} - A_{11}A_{26}\right) \quad \text{(C20)}$$

$$h_{26} = -A_{11}A_{66}\left(A_{11}A_{22} - A_{12}^2\right) + A_{16}^2\left(A_{11}A_{22} - 2A_{12}^2\right) + A_{11}A_{26}\left(2A_{12}A_{16} - A_{11}A_{26}\right) \quad \text{(C21)}$$

$$h_{66} = 2\left(A_{11}A_{26} - A_{12}A_{16}\right)\left(A_{11}A_{22} - A_{12}^2\right) \quad \text{(C22)}$$

Special Cases for $\mathcal{A}_0$ and $\mathcal{C}_1$

Simplifications to $\mathcal{A}_0$ and $\mathcal{C}_1$ are presented below for unbalanced and balanced, symmetric laminates and for balanced, unsymmetric laminates, that include the subclasses of general antisymmetric laminates, antisymmetric cross-ply laminates, and antisymmetric angle-ply laminates.

Unbalanced and balanced, symmetric laminates. For unbalanced, symmetric laminates, $A_{16} \neq 0$, $A_{26} \neq 0$, and $B_{11} = B_{12} = B_{22} = B_{16} = B_{26} = B_{66} = 0$. For this special case,

$$\mathcal{A}_0 = \left[\frac{\left(A_{11}A_{22} - A_{12}^2\right)\left(A_{11}A_{66} - A_{16}^2\right)}{A_{11}\left[\left(A_{11}A_{22} - A_{12}^2\right)A_{66} - A_{11}A_{26}^2 - A_{22}A_{16}^2 + 2A_{12}A_{16}A_{26}\right]}\right]^{1/4} \quad \text{(C23)}$$

which agrees with the corresponding equations given by Reuter[4], and

$$\mathcal{C}_1 = \frac{D_{16}\left(A_{12}A_{16} - A_{11}A_{26}\right)}{2h\left[D_{11}\left(A_{11}A_{66} - A_{16}^2\right)\right]^{1/2}}\Big[\left(A_{11}A_{22} - A_{12}^2\right)A_{66}$$

$$- A_{11}A_{26}^2 - A_{22}A_{16}^2 + 2A_{12}A_{16}A_{26}\Big]^{-1/2} \quad \text{(C24)}$$

For balanced, symmetric laminates, $A_{16} = A_{26} = 0$ in addition to the subscripted B-matrix constitutive terms. For this special case, $\mathcal{A}_0 = 1$ and $\mathcal{C}_1 = 0$.

Balanced, unsymmetric laminates. For balanced, unsymmetric laminates, $A_{16} = A_{26} = 0$, which yields the following simplified expressions

$$\varepsilon_0 = 1 - \frac{B_{11}^2}{A_{11}D_{11}} - \frac{B_{16}^2}{A_{66}D_{11}} \quad \text{(C25)}$$

$$\Lambda = \frac{A_{11}B_{12} - A_{12}B_{11}}{\sqrt{A_{11}D_{11}(A_{11}A_{22} - A_{12}^2)\varepsilon_0}} \quad \text{(C26)}$$

$$\mathcal{A}_0 = \sqrt[4]{\varepsilon_0}\left[1 + \Lambda\right]^{-1/2} \quad \text{(C27)}$$

$$\varepsilon_1 = -2\frac{B_{16}}{A_{66}h}\left[\frac{D_{16}}{D_{11}} - \frac{B_{11}B_{16}}{A_{11}D_{11}} - \frac{B_{16}B_{66}}{A_{66}D_{11}}\right] \quad \text{(C28)}$$

$$\mathcal{C}_1 = \frac{1}{4(1+\Lambda)}\left[\frac{\varepsilon_1}{\varepsilon_0}(1+2\Lambda) + \frac{2B_{16}\left(A_{11}B_{26} - A_{12}B_{16}\right)}{A_{66}h\sqrt{A_{11}D_{11}\left(A_{11}A_{22} - A_{12}^2\right)\varepsilon_0}}\right] \quad \text{(C29)}$$

For the subclass of balanced, antisymmetric laminates, $D_{16} = D_{26} = 0$ in addition to the shear-extensional coupling terms, which yields the following simplification

$$\varepsilon_1 = \frac{2B_{16}^2}{A_{66}D_{11}h}\left[\frac{B_{11}}{A_{11}} + \frac{B_{66}}{A_{66}}\right] \quad \text{(C30)}$$

that is applied to Eq. (C29). For the subclass of (balanced) antisymmetric cross-ply laminates, $B_{12} = B_{16} = B_{26} = B_{66} = 0$, $B_{22} = -B_{11}$, and $D_{16} = D_{26} = 0$ in addition to the shear-extensional coupling terms. For this special case, $\mathcal{C}_1 = 0$ and

$$\mathcal{A}_0 = \sqrt[4]{\varepsilon_0}\left[1 - \frac{A_{12}B_{11}}{\sqrt{A_{11}D_{11}(A_{11}A_{22} - A_{12}^2)\varepsilon_0}}\right]^{-1/2} \quad \text{(C31)}$$

where

$$\varepsilon_0 = 1 - \frac{B_{11}^2}{A_{11}D_{11}} \quad \text{(C32)}$$

For the subclass of balanced, antisymmetric angle-ply laminates, $B_{11} = B_{12} = B_{22} = B_{66} = 0$ and $D_{16} = D_{26} = 0$ in addition to the shear-extensional coupling terms. For this special case, $\mathcal{A}_0 = \sqrt[4]{\varepsilon_0}$ where

$$\varepsilon_0 = 1 - \frac{B_{16}^2}{A_{66}D_{11}} \quad \text{(C33)}$$

which agrees with the corresponding equations given by Reuter[4], and

$$\mathcal{C}_1 = \frac{B_{16}\left(A_{11}B_{26} - A_{12}B_{16}\right)}{2A_{66}h\sqrt{A_{11}D_{11}\left(A_{11}A_{22} - A_{12}^2\right)\varepsilon_0}} \quad \text{(C34)}$$

Further simplifications can be made to Eqs. (C31) and (C32) for [0/90/.../90] antisymmetric-cross-ply-laminate shell walls with an even number of layers that have identical material properties. For these laminates, the plies are specially orthotropic and their principal material directions are oriented at 0 deg and 90 deg to the cylinder axes in an alternating manner. In particular, the major principal axes of the odd-numbered and even-numbered plies are aligned with the x- and θ-axis, respectively, with the first ply in the stacking sequence located at the inner surface of the cylinder. Moreover, the odd-numbered plies have the same thickness and the even-numbered plies have the same thickness, but these two thicknesses are, in general, different. The laminate stiffnesses are given in Ref. 18 (see pp. 224-226) in terms of the number of layers N, the thickness ratio M, the ratio of the principal elastic moduli $F = \frac{E_2}{E_1}$, for which $0 < F \le 1$, and the reduced, plane-stress lamina stiffnesses. The thickness ratio is defined by

$$M = \sum_{k=1,3,\ldots}^{N-1} t_{(k)} \div \sum_{k=2,4,\ldots}^{N} t_{(k)} = \frac{t_{(1)}}{t_{(2)}} \quad \text{(C35)}$$

where $t_{(k)}$ denotes the thickness of the k^{th} ply and

$$h = \sum_{k=1,3,\ldots}^{N-1} t_{(k)} + \sum_{k=2,4,\ldots}^{N} t_{(k)} = \frac{N}{2}\left(t_{(1)} + t_{(2)}\right) \quad \text{(C36)}$$

is the total laminate thickness. For the antisymmetric cross-ply laminates, $t_{(1)}$ and $t_{(2)}$ are the thicknesses of the 0-deg and 90-deg layers, respectively, and are denoted herein by t_0 and t_{90}, respectively. Substituting the nonzero laminate stiffness expressions for this class of antisymmetric cross-ply laminates that are given in Ref. 18 into Eqs. (21), (C31), and (C32) yields

$$\mathcal{O} = \left[\frac{[1-(1-F)Q](M+1)(M+F)}{(M+F)(1+MF)-[(1+M)Fv_{12}]^2} \right]^{1/4} \quad \text{(C37)}$$

$$\mathcal{A}_0 = \sqrt[4]{e_0}\left[1 + \frac{\sqrt{12}\, MF(1-F)\, v_{12}}{N\Sigma} \right]^{-1/2} \quad \text{(C38a)}$$

where

$$\Sigma = \left[[1-(1-F)Q](M+1)(M+F)\times \{(M+F)(1+MF)-[(M+1)Fv_{12}]^2\}e_0 \right]^{1/2} \quad \text{(C38b)}$$

$$e_0 = 1 - \frac{12M^2(1-F)^2}{N^2(M+1)^3(M+F)[1-(1-F)Q]} \quad \text{(C39)}$$

$$Q = \frac{1}{1+M} + \frac{8M(M-1)}{N^2(M+1)^3} \quad \text{(C40)}$$

and v_{12} is the major Poisson's ratio. For the special, but practical, case of regular antisymmetric cross-ply lamination, all plies have the same thickness and Eqs. (C37) - (C39) reduce to

$$\mathcal{O} = \left[1 - \left(\frac{(2Fv_{12}}{1+F} \right)^2 \right]^{-1/4} \quad \text{(C41)}$$

$$\mathcal{A}_0 = \sqrt[4]{e_0}\left[1 + \frac{\sqrt{12}\, v_{12} F(1-F)}{N(1+F)\sqrt{[(1+F)^2-(2Fv_{12})^2]e_0}} \right]^{-1/2} \quad \text{(C42)}$$

$$e_0 = 1 - \frac{3}{N^2}\left(\frac{1-F}{1+F} \right)^2 \quad \text{(C43)}$$

References

[1]Kraus, H., *Thin Elastic Shells - An Introduction to the Theoretical Foundations and the Analysis of Their Static and Dynamic Behavior,* John Wiley and Sons, Inc., 1967, pp. 131-142.

[2]Pagano, N. J. and Whitney, J. M., "Geometric Design of Composite Cylindrical Characterization Specimens," *Journal of Composite Materials*, Vol. 4, July 1970, pp. 360-378.

[3]Dong, S. B., Pister, K. S., and Taylor, R. L., "On the Theory of Laminated Anisotropic Shells and Plates," *Journal of the Aerospace Sciences*, August 1962, pp. 969-975.

[4]Reuter, R. C., Jr., "Analysis of Shells Under Internal Pressure," *Journal of Composite Materials*, Vol. 6, January 1972, pp. 94-113.

[5]Hennemann, Jose C. F., "Effect of Prebuckling Deformations on Buckling of Laminated Composite Circular Cylindrical Shells," Ph. D. Dissertation, Civil and Mechanical Engineering Dept., Southern Methodist University, Dallas, Texas, 1975.

[6]Cheng, S. and He, F. B., "Theory of Orthotropic and Composite Cylindrical Shells, Accurate and Simple Fourth-Order Governing Equations," *Journal of Applied Mechanics*, Vol. 51, December 1984, pp. 736-744.

[7]Sayir, M., "Edge Effects in Rotationally Symmetric Composite Shells," *Local Effects in the Analysis of Structures*, editied by Pierre Ladeveze, Studies in Applied Mechanics 12, Elsevier Science Publishing Co., Inc., 1985, pp. 161-180.

[8]Chaudhuri, R. A., Balaraman, K., and Kunukkasseril, V. X., "Arbitrarily Laminated, Anisotropic Cylindrical Shell Under Internal Pressure," *AIAA Journal*, Vol. 24, No. 11, November 1986, pp. 1851-1858.

[9]Butler, T. A. and Hyer, M. W., "The Structural Response of Unsymmetrically Laminated Composite Cylinders," Dept. of Mechanical Engineering, Technical Report 89-2, The University of Maryland, August 1989.

[10]Hyer, M. W. and Paraska, P. J., "Innovative Design of Composite Structures: Axisymmetric Deformations of Unsymmetrically Laminated Cylinders Loaded in Axial Compression," Dept. of Engineering Science and Mechanics, VPI-E-90-10 Report, VA Tech, June, 1990.

[11]Paraska, P. J., "Axisymmetric Deformations and Stresses of Unsymmetrically Laminated Composite Cylinders in Axial Compression with Thermally-Induced Preloading Effects," Carderock Division, Naval Surface Warfare Center, Carderockdiv-U-SSm-65-93/03 Report, March, 1993.

[12]Vinson, J. R., "Composite Shell Structures and Their Behavior," Proceedings of the AIAA/ASME/ASCE/AHS/ASC 38th Structures, Structural Dynamics, and Materials Conference, Kissimmee, Florida, April 7-10, 1997, pp. 2400-2406.

[13]McDevitt, T. J. and Simmonds, J. G., "Reduction of the Sanders-Koiter Equations for Fully Anisotropic Circular Cylindrical Shells to Two Coupled Equations for a Stress and a Curvature Function," *Journal of Applied Mechanics*, Vol. 66, September 1999, pp. 593-597.

[14]Flugge, W., *Stresses in Shells*, Springer-Verlag, Berlin, 1967.

[15]Goldenveizer, A. L., *Theory of Thin Elastic Shells*, Pergamon, New York, 1961.

[16] Sanders, J. L., Jr., "An Improved First-Approximation Theory for Thin Shells," NASA TR R-24, February 1959.

[17]Koiter, W. T., "A Consistent First Approximation in the General Theory of Thin Elastic Shells," *The Theory of Thin Elastic Shells, Proceedings of the IUTAM Symposium*, Delft, North-Holland, Amsterdam, The Netherlands, 1960, pp. 12-33.

[18] Jones, R. M., *Mechanics of Composite Materials*, 2nd ed., Taylor and Francis, 1999.

[19]Zwillinger, D., ed., *Standard Mathematical Tables and Formulae*, 30th ed., CRC Press, 1996, pp. 133-134.

[20]Nemeth, M. P. and Anderson, M. S., "Axisymmetric Shell Analysis of the Space Shuttle Solid Rocket Booster Field Joint," NASA TP 3033, January, 1991.

[21]Nemeth, M. P. and Anderson, M. S., "Axisymmetric Shell Analysis of the Space Shuttle Solid Rocket Booster Field Joint," *Journal of Spacecraft and Rockets*, Vol. 27, No. 1, Jan.-Feb., 1990, pp. 85-92.

[22]Jaunky, N. and Knight, N. F., Jr., "An Assessment of Shell Theories for Buckling of Circular Cylindrical Laminated Composite Panels Loaded in Axial Compression," *International J. of Solids and Structures*, Vol. 36, 1999, pp. 3799-3820.

Table 1: Lamina properties.

Lamina property*	Material Systems								
	Boron-Al	S-glass-epoxy	Kevlar 49-epoxy	IM7/5260	AS4/3502	AS4/3501-6	Boron-epoxy	IM7/PETI-5	P-100/3502
E_1, Msi	33	7.5	11.02	22.1	18.5	20.01	29.58	20.35	53.5
E_2, Msi	21	1.7	0.8	1.457	1.64	1.30	2.68	1.16	0.73
ν_{12}	0.23	0.25	0.34	0.258	0.30	0.30	0.23	0.29	0.31
G_{12}, Msi	7.0	0.80	0.33	0.860	0.87	1.03	0.81	0.61	0.76
$\alpha_1 \times 10^6$/°F	3.2	3.5	-2.22	0.0125	0.25	-0.167	3.38	-0.14	-0.64
$\alpha_2 \times 10^6$/°F	11.0	11.0	43.89	14.91	16.2	15.6	16.83	16.85	17.2

* The subscripts 1 and 2 denote the longitudinal (fiber) and transverse (matrix) directions of a specially orthotropic lamina, respectively.

Table 2: Comparison of results for specially orthotropic materials with Ref. 6.

Material Systems*	E_2/E_1	ν_{12}	θ	$\mathcal{R}e(\mu)$, Ref. 6‡	$\mathcal{R}e(\mu)$, Present study‡
Boron-epoxy	0.100	0.30	1.782	2.796-2.805	2.806
Glass-epoxy	0.333	0.25	1.323	3.757-3.779	3.779
Graphite-epoxy	0.250	0.25	2.516	1.984-1.987	1.987

* The subscripts 1 and 2 denote the major and minor principal directions, respectively, of the specially orthotropic materials defined in Ref. 6.

‡ The quantity $\mathcal{R}e(\mu)$ is defined by Eq. (37).

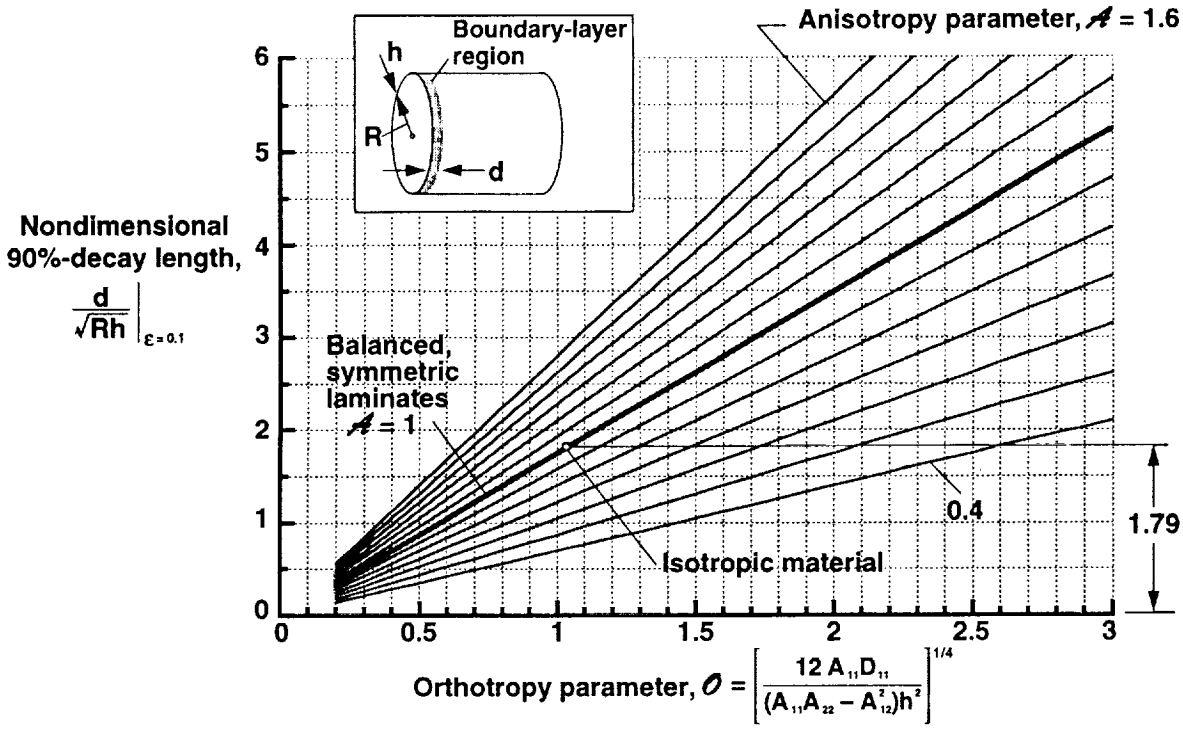

Fig. 1 Nondimensional 90%-decay length for symmetrically and unsymmetrically laminated cylinders, as a function of laminate orthotropy.

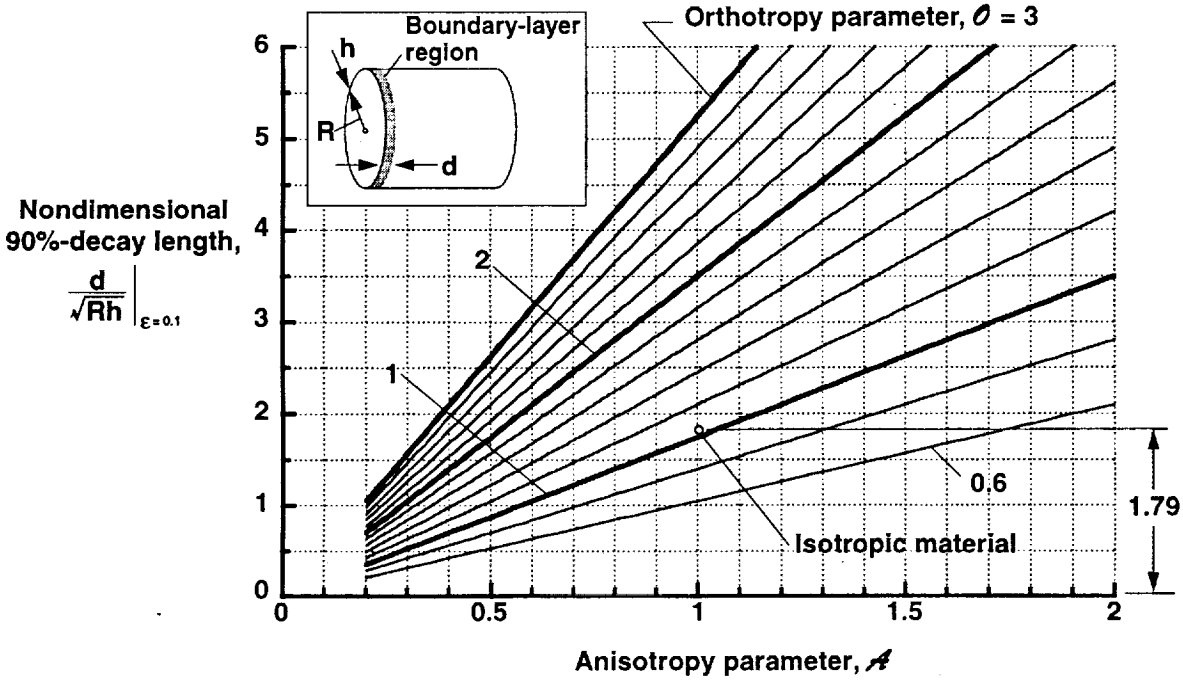

Fig. 2 Nondimensional 90%-decay length for symmetrically and unsymmetrically laminated cylinders, as a function of laminate anisotropy.

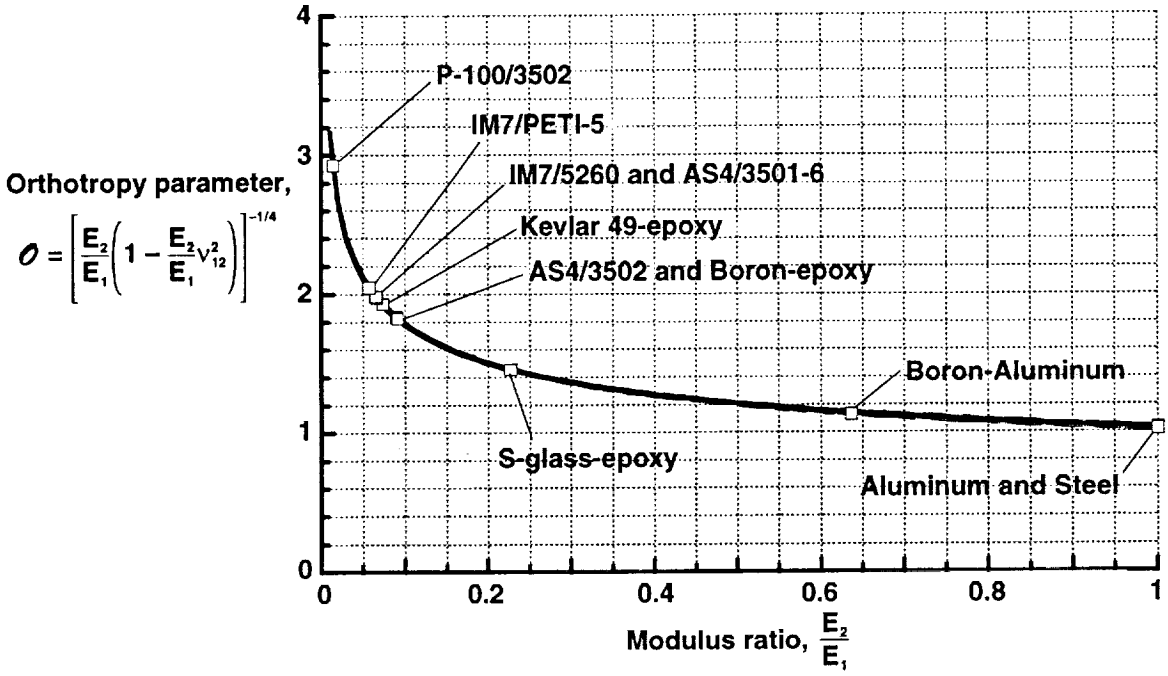

Fig. 3 Effect of lamina material properties on nondimensional orthotropy parameter for single-ply, homogeneous, specially orthotropic laminates ($0.2 \le \nu_{12} \le 0.35$).

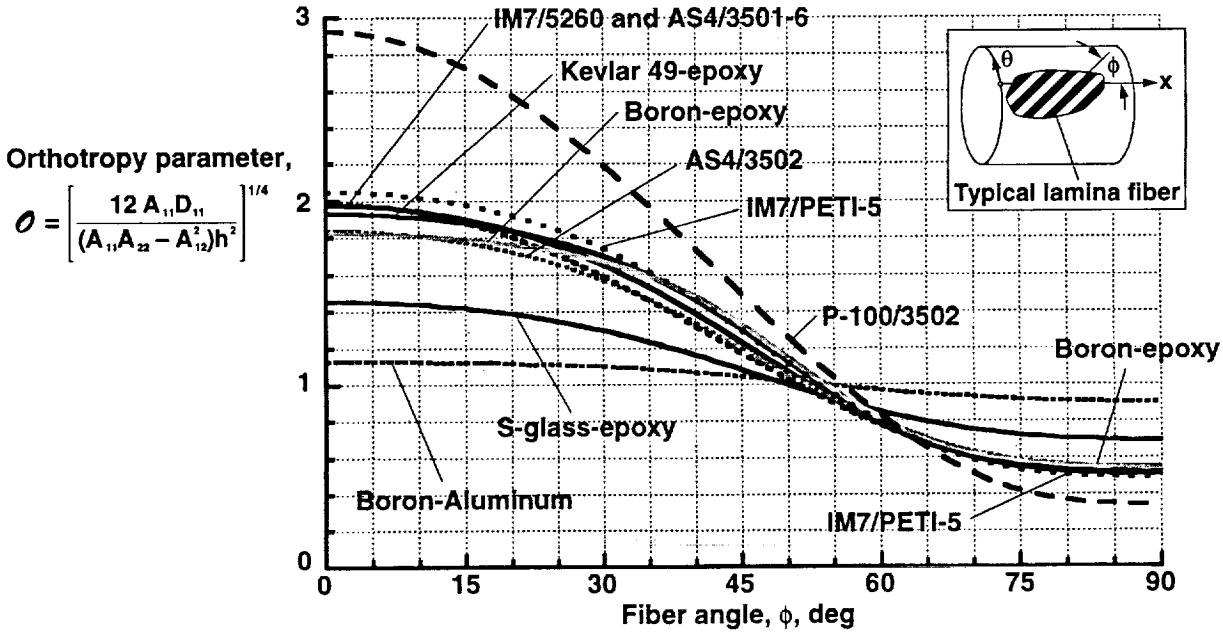

Fig. 4 Effect of lamina material properties on nondimensional orthotropy parameter for $[(\pm\phi)_m]_s$, $[(+\phi)_{2m}]_s$, and $[(\pm\phi)_m]_T$ laminates (m = 1, 2, ...).

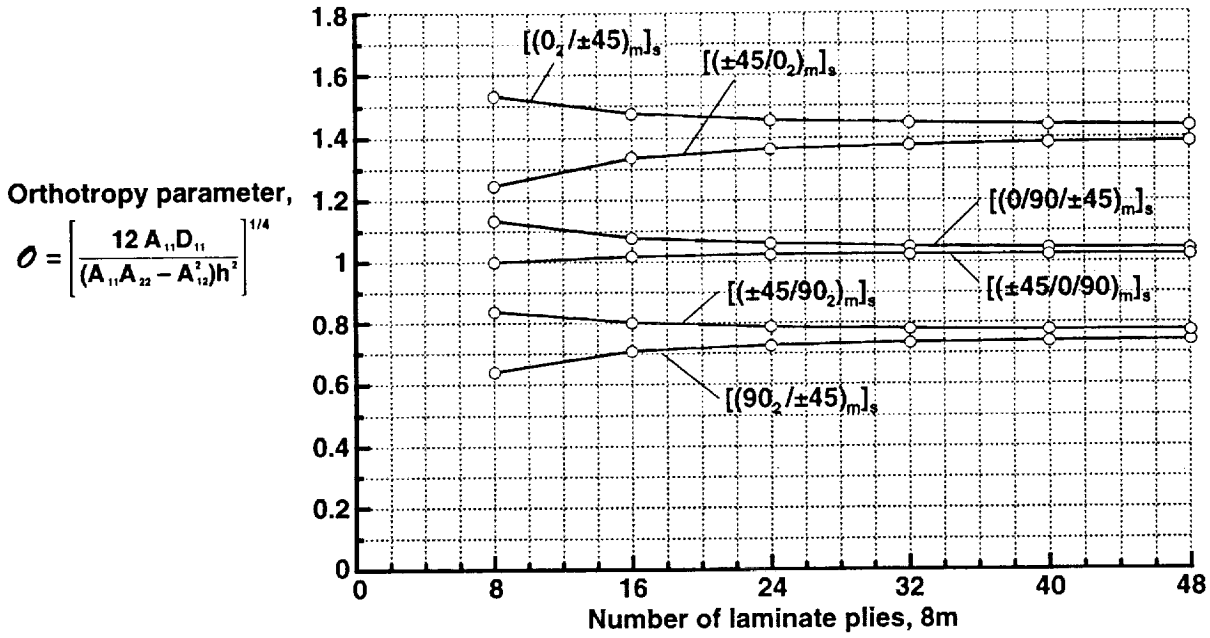

Fig. 5 Nondimensional orthotropy parameter for typical laminates made of IM7/5260 material.

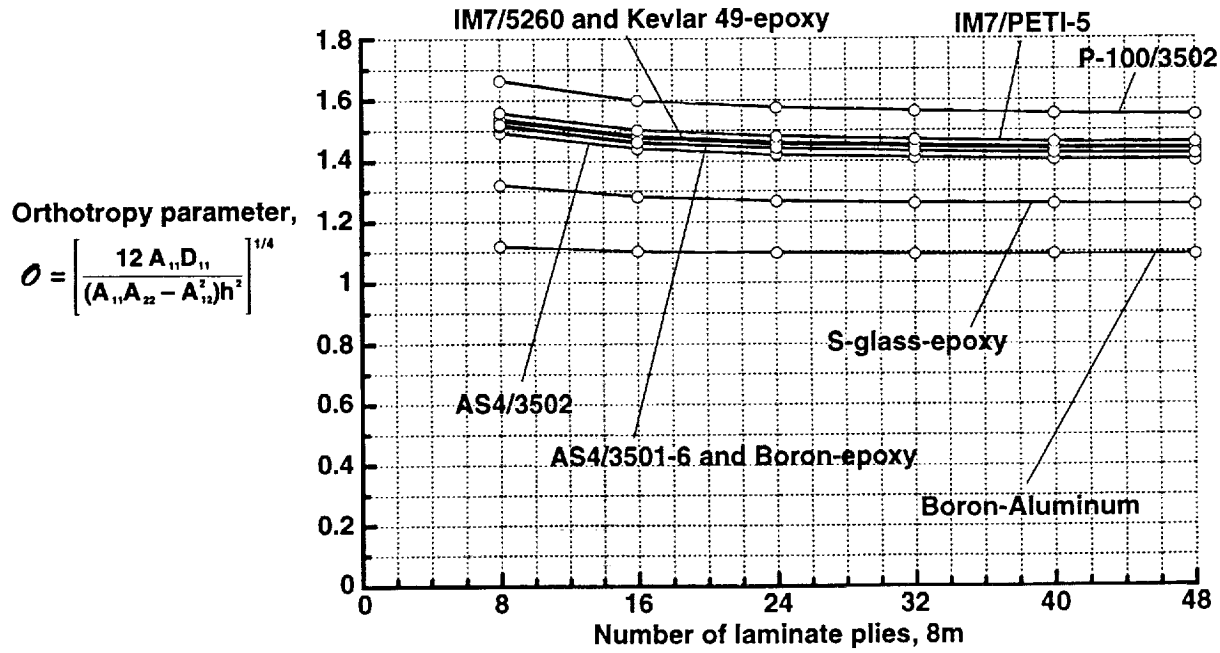

Fig. 6 Effect of lamina material properties on nondimensional orthotropy parameter for $[(0_2/\pm45)_m]_s$ laminates.

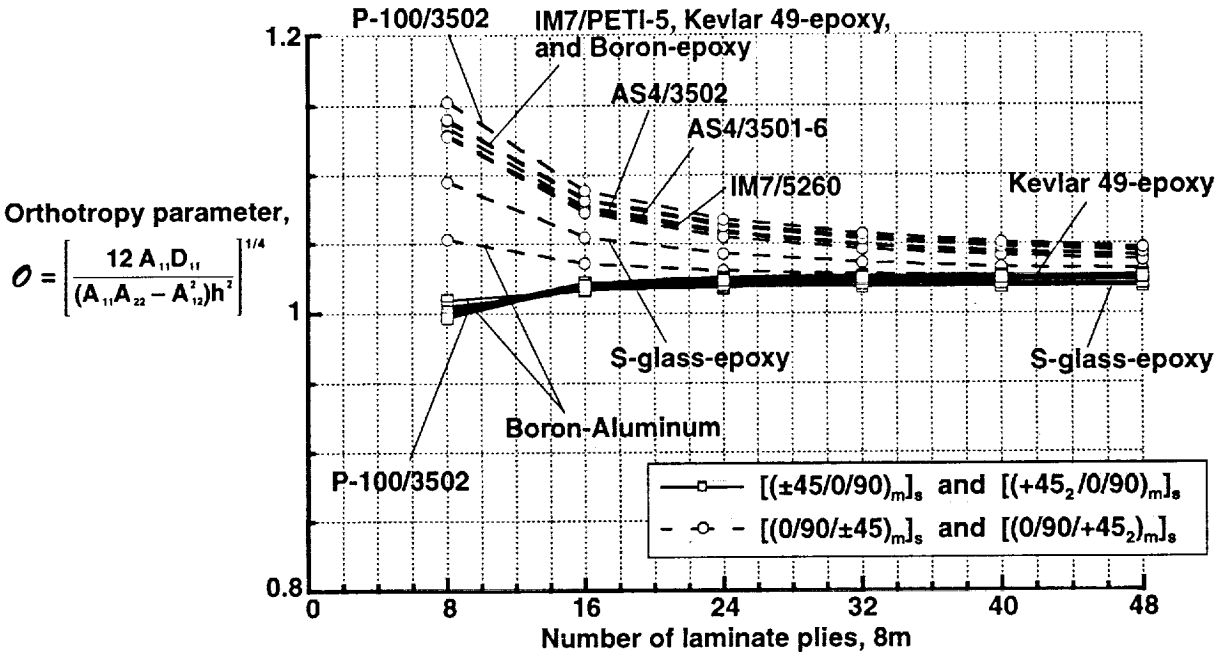

Fig. 7 Effect of lamina material properties on nondimensional orthotropy parameter for quasi-isotropic laminates and similar unbalanced laminates.

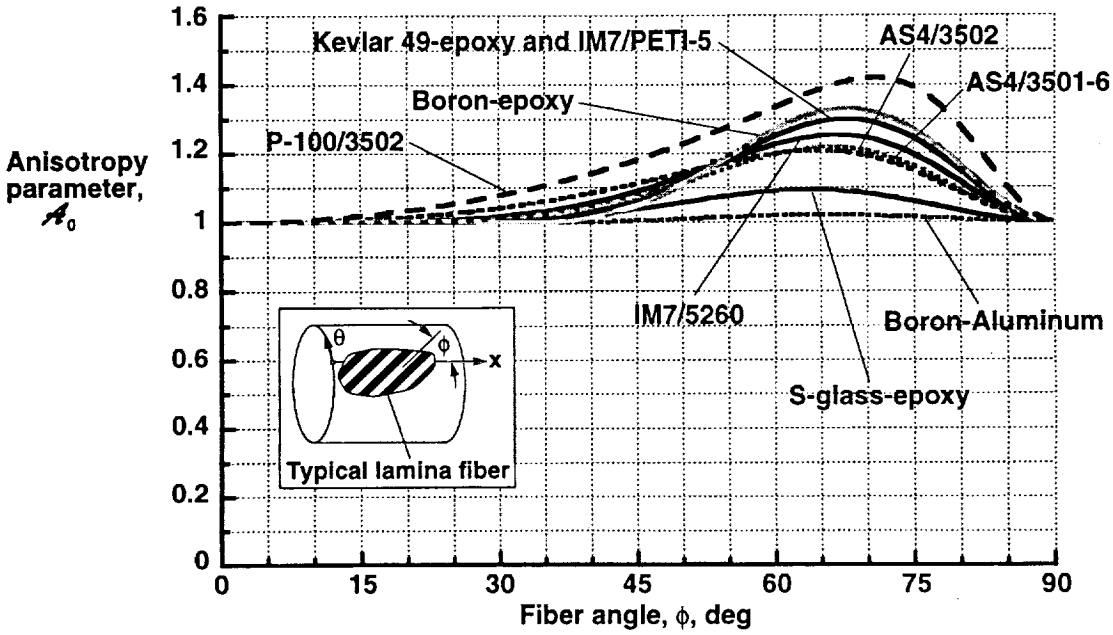

Fig. 8 Effect of lamina material properties on nondimensional anisotropy parameter for $[(+\phi)_{2m}]_s$ laminates (m = 1, 2, ...).

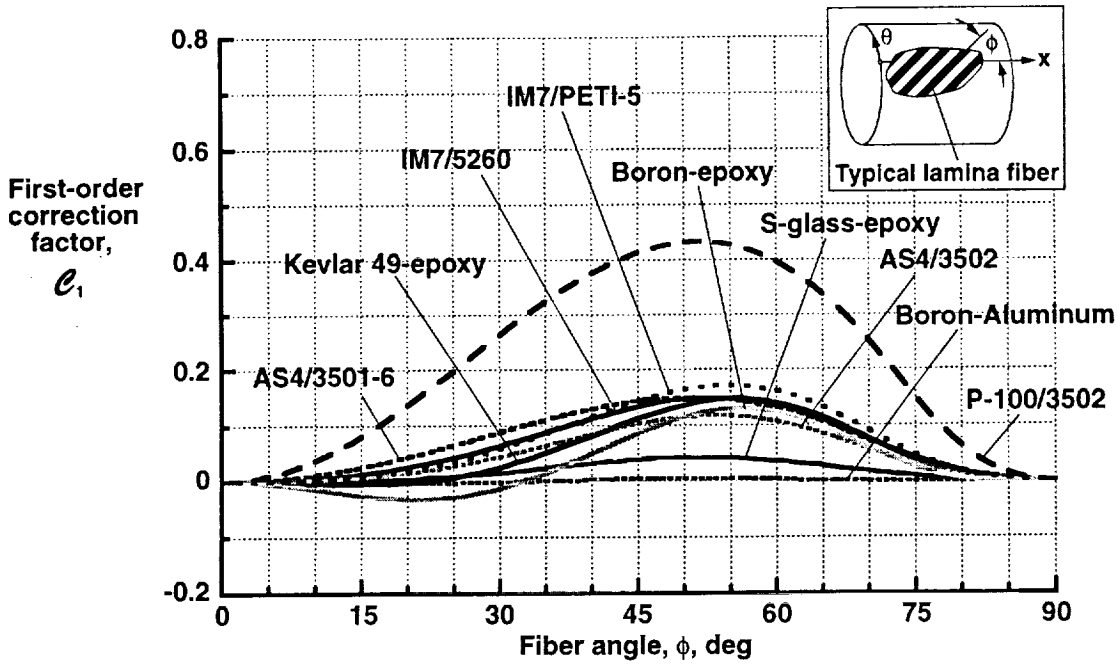

Fig. 9 Effect of lamina material properties on nondimensional first-order correction factor for $[(+\phi)_{2m}]_s$ laminates (m = 1, 2, ...).

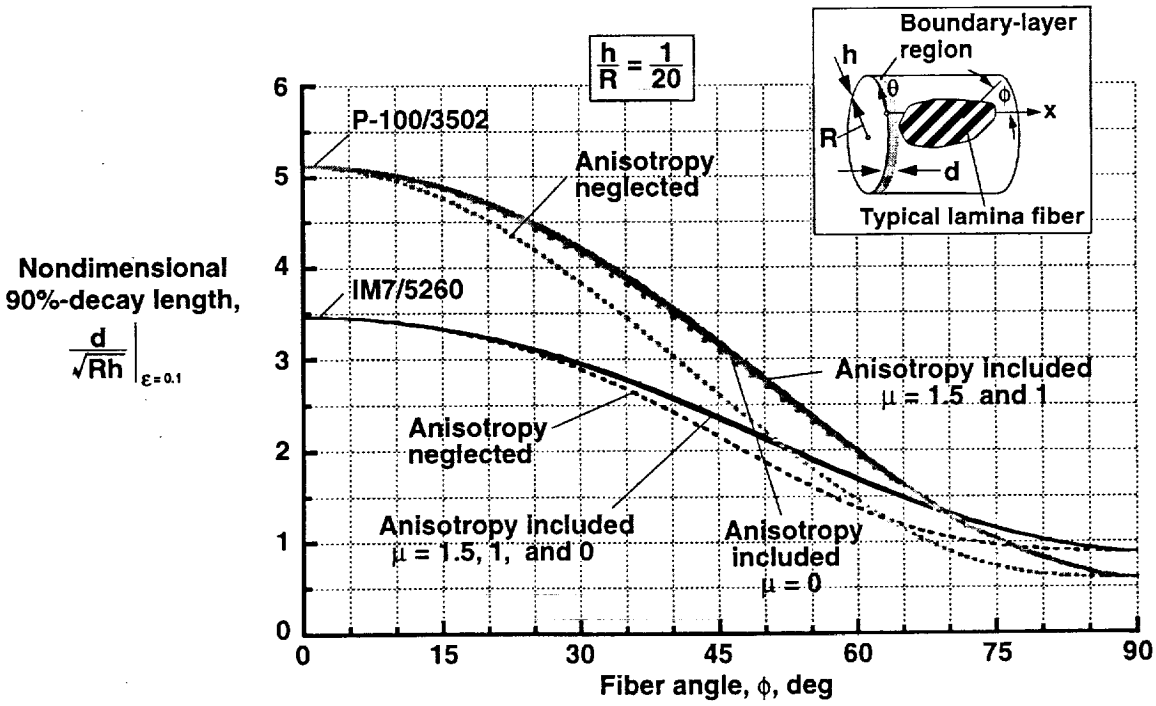

Fig. 10 Nondimensional 90%-decay length for $[(+\phi)_{2m}]_s$ laminates made of IM7/5260 graphite-bismaleimide and P-100/3502 pitch-epoxy material (h/R = 1/20; m = 1, 2, ...).

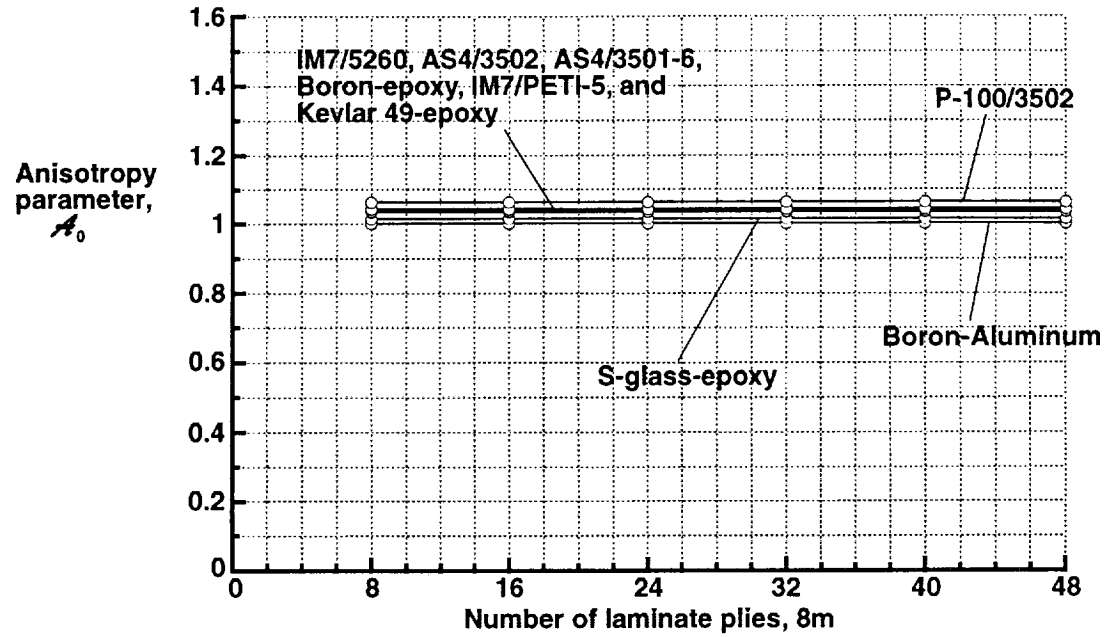

Fig. 11 Effect of lamina material properties on nondimensional anisotropy parameter for $[(0/90/+45_2)_m]_s$ and $[(+45_2/0/90)_m]_s$ laminates.

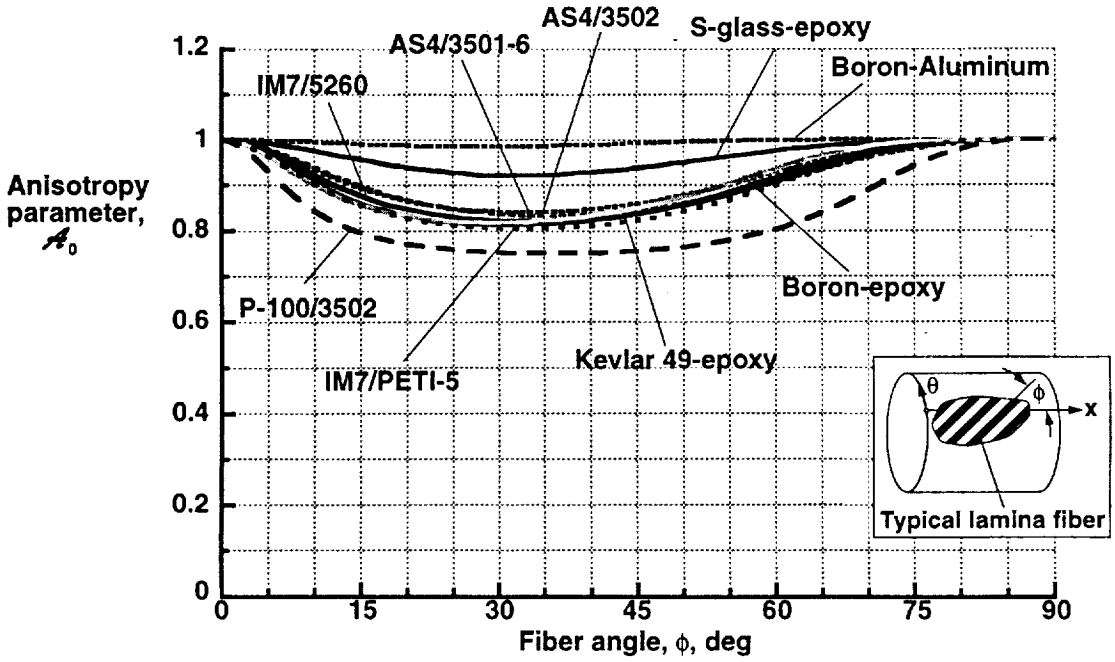

Fig. 12 Effect of lamina material properties on nondimensional anisotropy parameter for $[\pm\phi]_T$ laminates.

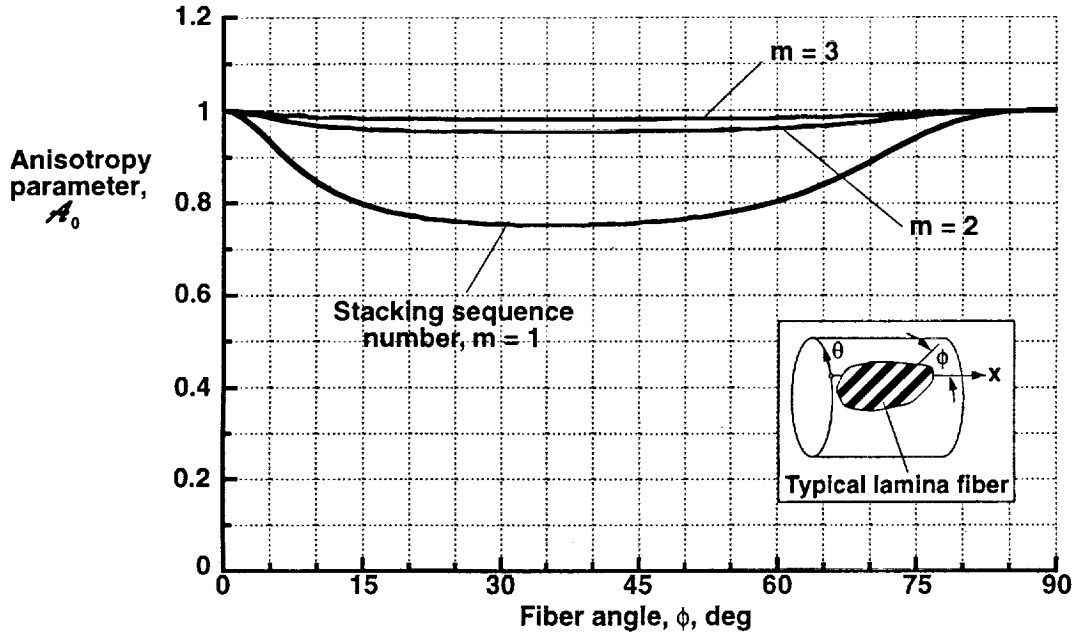

Fig. 13 Effect of stacking sequence number on nondimensional anisotropy parameter for $[(\pm\phi)_m]_T$ laminates made of P-100/3502 pitch-epoxy material.

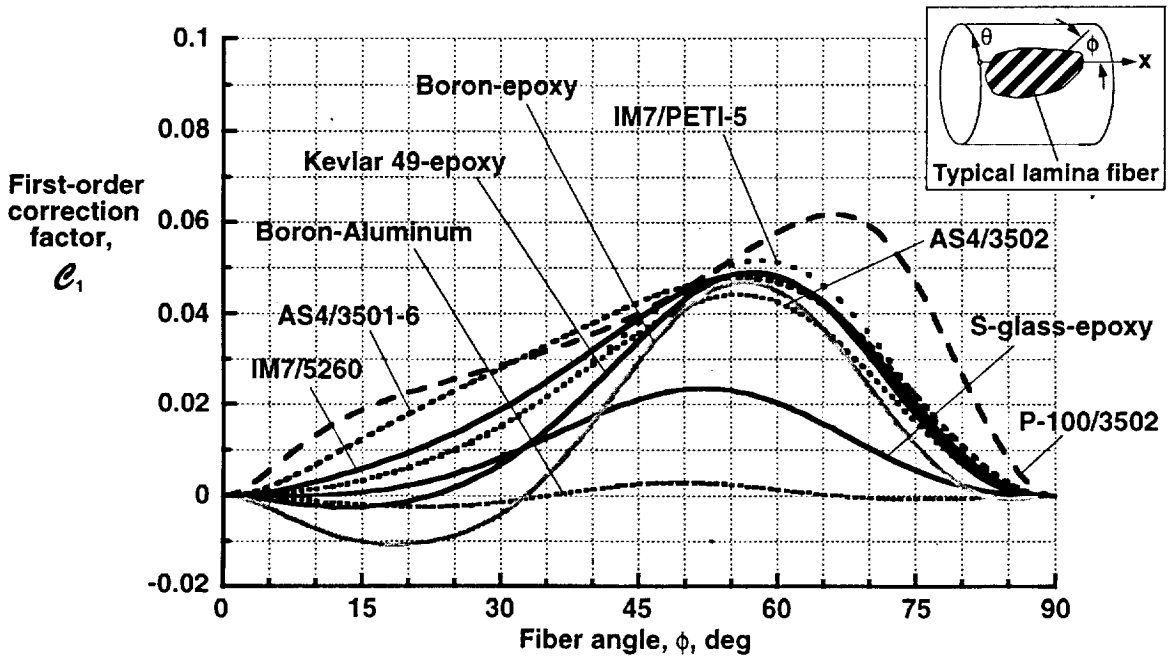

Fig. 14 Effect of lamina material properties on nondimensional first-order correction factor for $[\pm\phi]_T$ laminates.

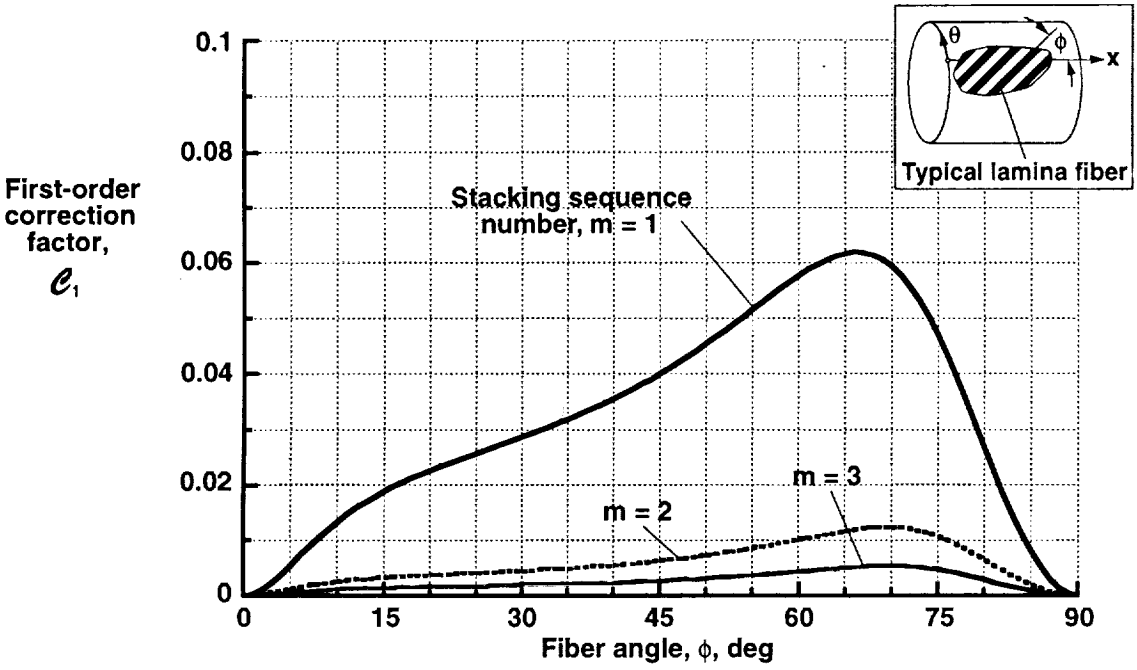

Fig. 15 Effect of stacking sequence number on nondimensional first-order correction factor for $[(\pm\phi)_m]_T$ laminates made of P-100/3502 pitch-epoxy material.

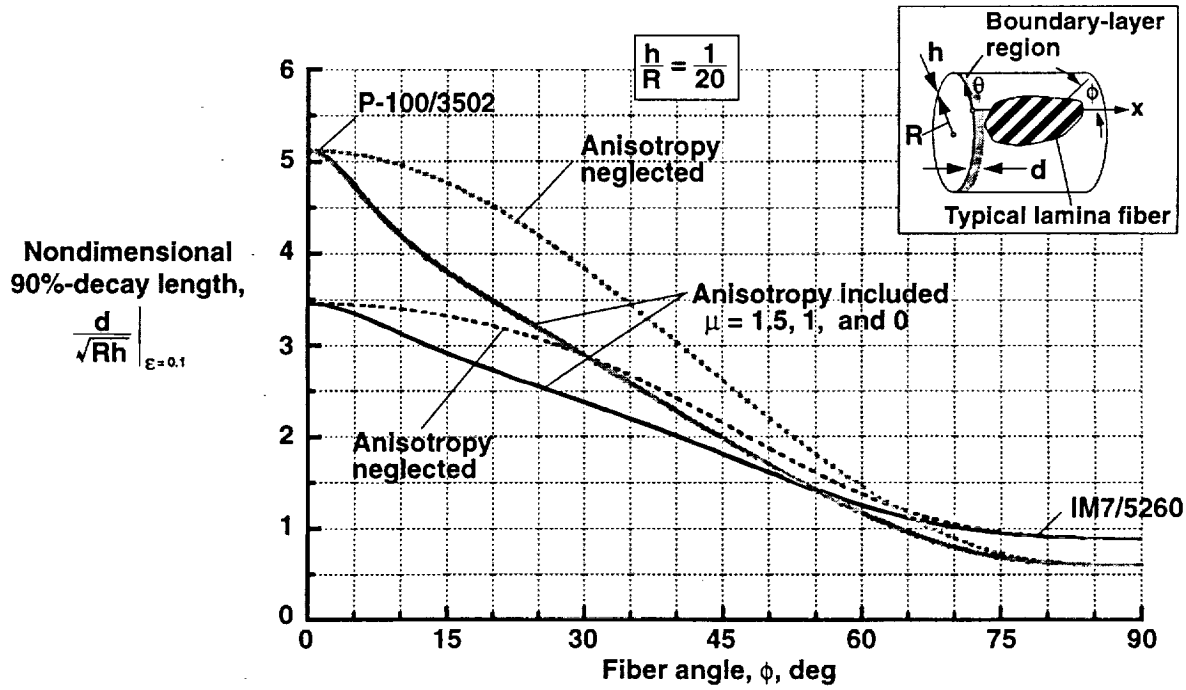

Fig. 16 Nondimensional 90%-decay length for $[\pm\phi]_T$ laminates made of IM7/5260 graphite-bismaleimide and P-100/3502 pitch-epoxy material (h/R = 1/20).

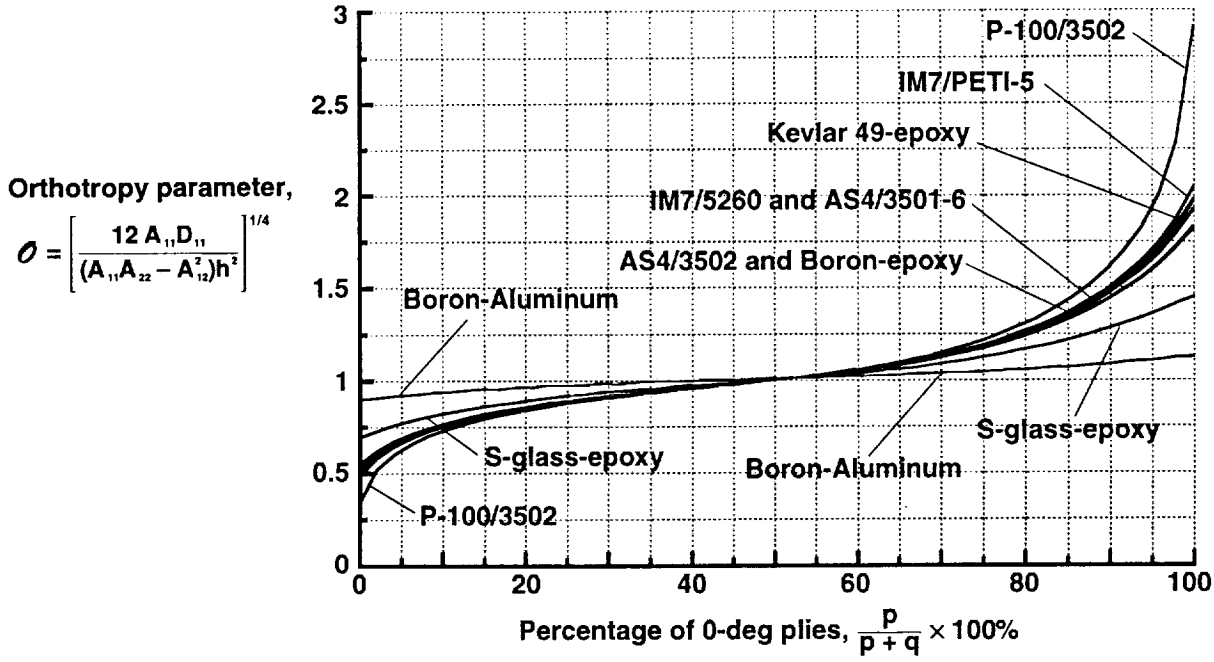

Fig. 17 Effect of lamina material properties on nondimensional orthotropy parameter for $[0_p/90_q]_T$ laminates.

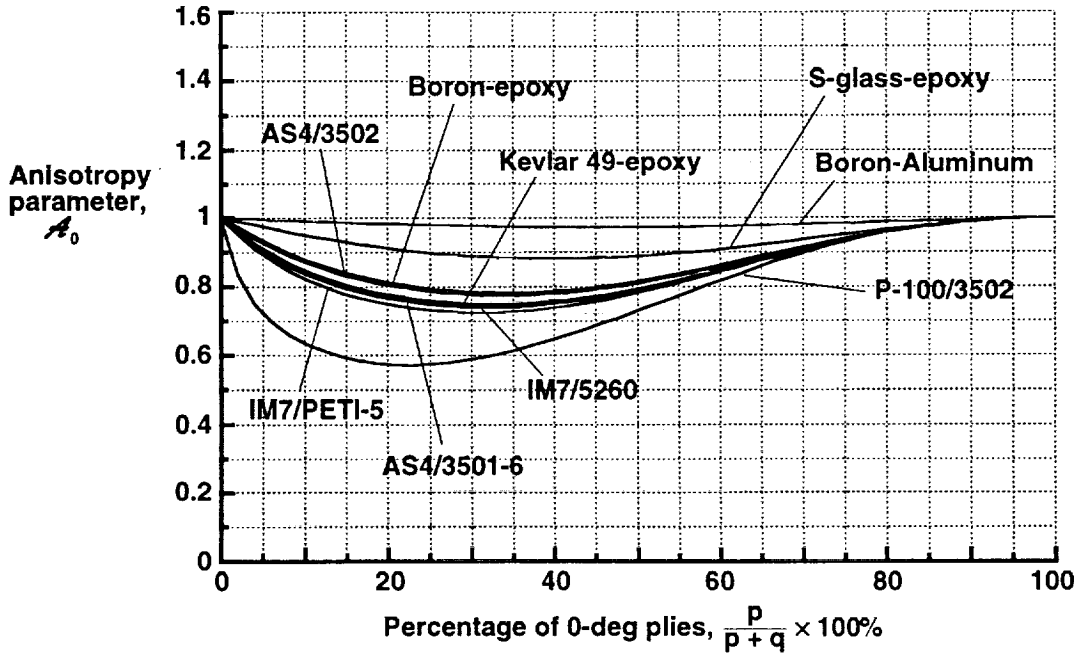

Fig. 18 Effect of lamina material properties on nondimensional anisotropy parameter for $[0_p/90_q]_T$ laminates.

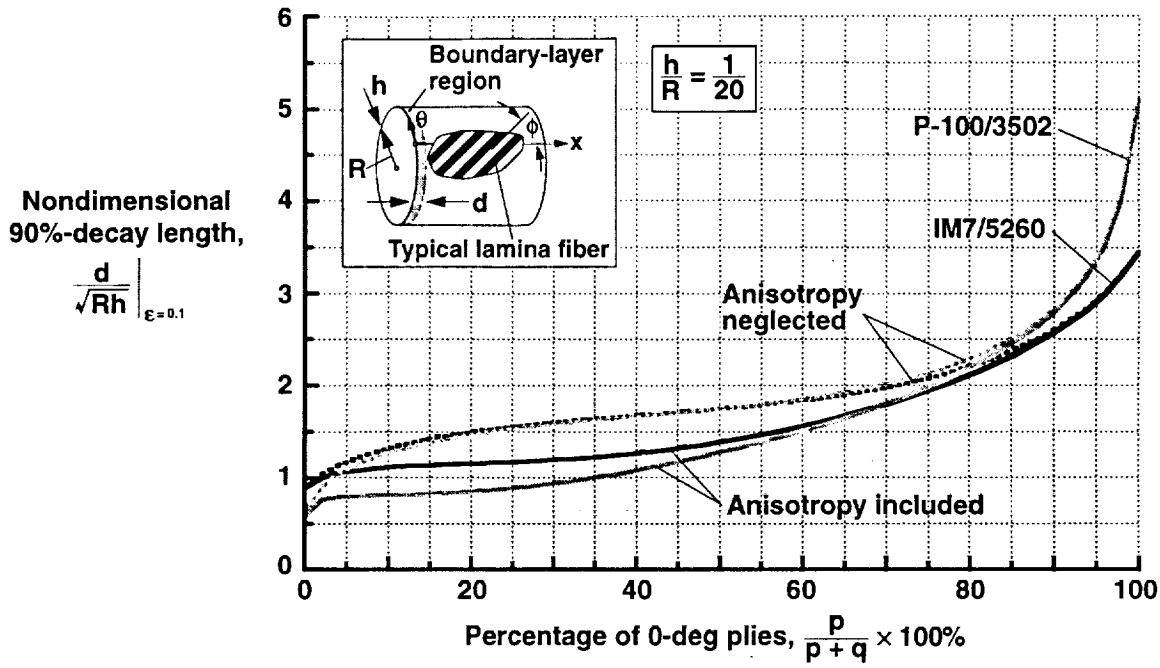

Fig. 19 Nondimensional 90%-decay length for $[0_p/90_q]_T$ laminates made of IM7/5260 graphite-bismaleimide and P-100/3502 pitch-epoxy material (h/R = 1/20).

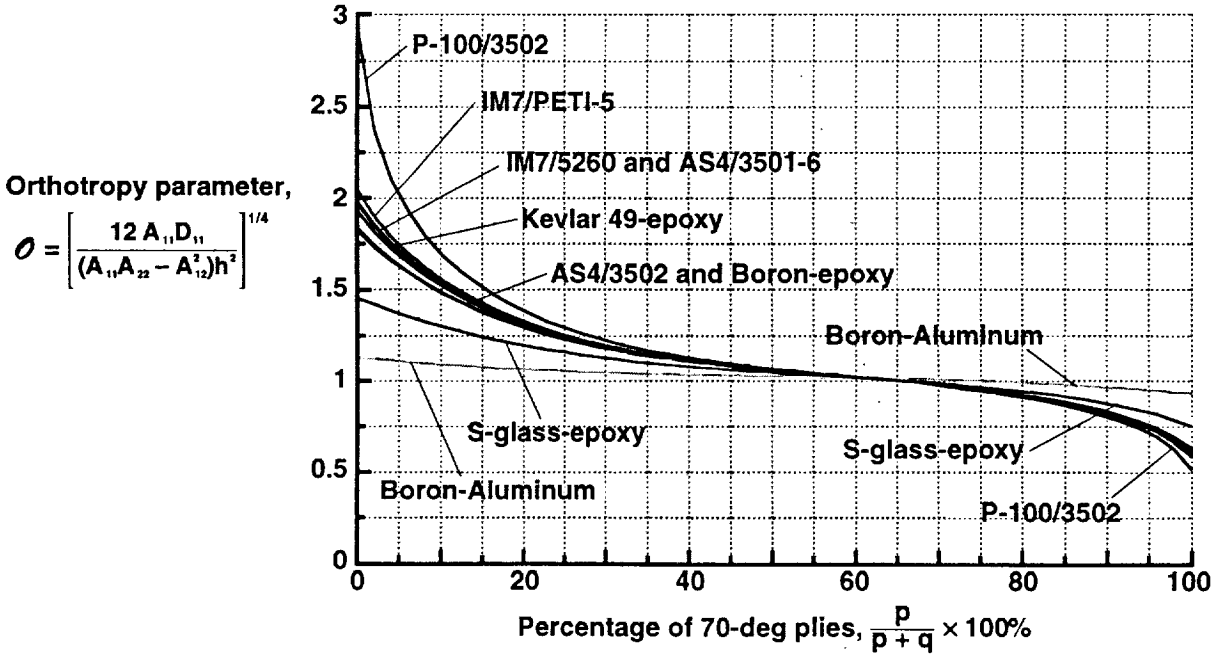

Fig. 20 Effect of lamina material properties on nondimensional orthotropy parameter for $[70_p/0_q]_T$ laminates.

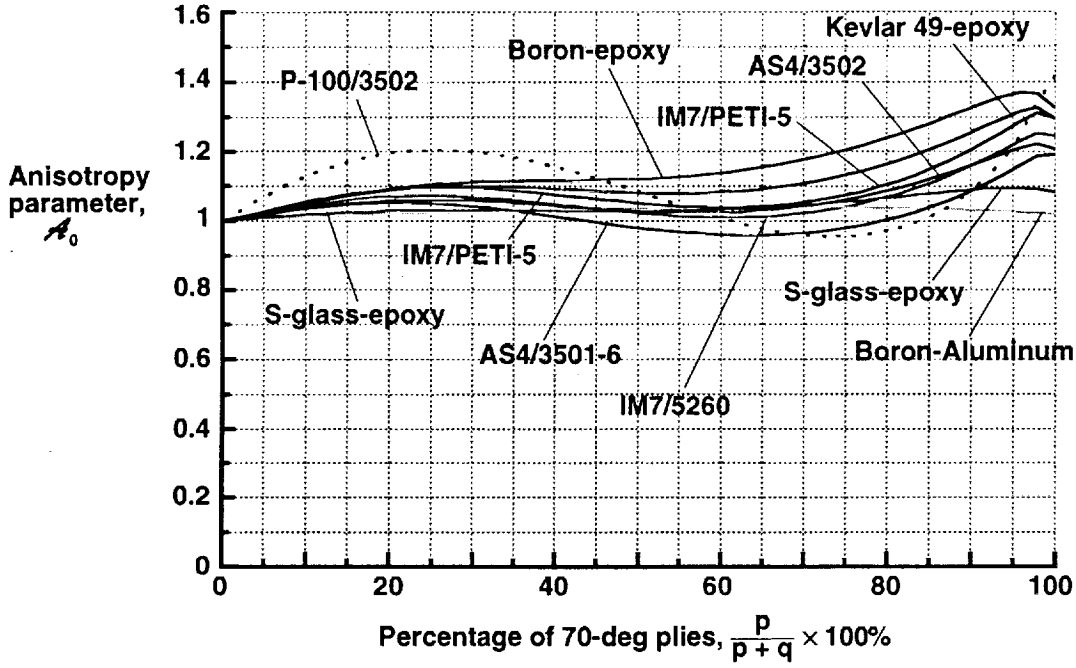

Fig. 21 Effect of lamina material properties on nondimensional anisotropy parameter for $[70_p/0_q]_T$ laminates.

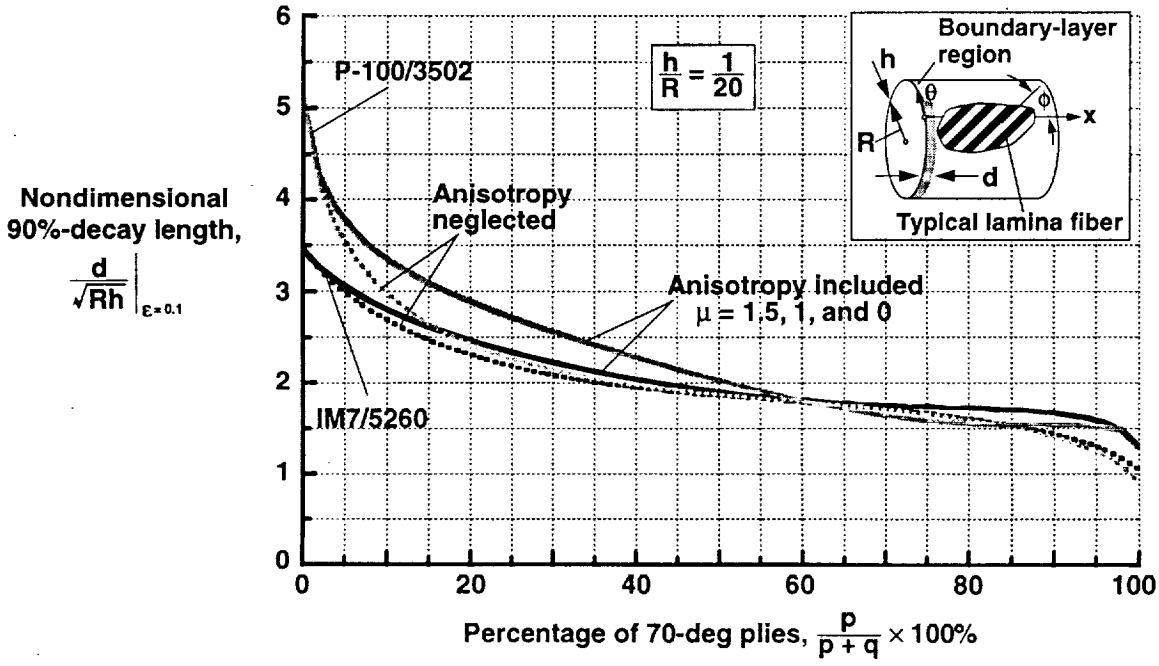

Fig. 22 Nondimensional 90%-decay length for $[70_p/0_q]_T$ laminates made of IM7/5260 graphite-bismaleimide and P-100/3502 pitch-epoxy material (h/R = 1/20).